2 On the remote sensing and radiative properties of cirrus

Anthony J. Baran

2.1 Introduction

Imagine an evening sky just before sunset as one gazes into the dark blue sky whilst lying in a country field surrounded by bird song, there often appears high in the sky wispy thin fibrous clouds. These innocuous-looking clouds are called cirrus. A non-specialist might be forgiven for thinking that such insubstantial-looking clouds are unimportant to the climate system. In fact, nothing could be further from the truth, as this chapter will demonstrate.

Cirrus is high-level cloud and appears at altitudes usually greater than about 6 km occurring at all latitudes and during all seasons (Wylie et al., 1994). Cirrus can cover substantial parts of the Earth's surface; recent estimates suggest the coverage to be 20–30% with 60–70% coverage in the tropics (Liou, 1986; Hartmann et al., 1992; Wylie et al., 1994). With such a spatial and temporal coverage cirrus has an important impact on the Earth atmosphere radiative balance (Stephens and Webster, 1981; Mitchell et al., 1989; Liou and Takano, 1994; Lohmann and Roeckner, 1995; Donner et al., 1997; Kristjánsson et al., 2000; Hong et al., 2006; Edwards et al., 2007). This impact can manifest itself in several ways. Cirrus exists at low temperatures and is optically thin high-level cloud, which generally transmit solar radiation and absorb long-wave radiation. Since cirrus is cold little infrared radiation is emitted back to space, thereby warming the Earth's surface, this is a positive feedback. However, ice cloud associated with deep convection or fronts can reflect significant amounts of solar radiation back to space, thereby tending to cool the Earth's surface, this is a negative feedback. In the paper by Zhang et al. (1999) it is shown that the net radiative forcing of cirrus can vary for a fixed optical depth (i.e., the cloud extinction multiplied by its vertical geometric depth) between net warming and net cooling by changing the size of ice crystals from large to small, respectively. The overall sign of the net cirrus radiative forcing is crucial to determine if climate models are to realistically simulate future climate change (IPCC, 2001). In order to achieve this it is necessary to understand the basic microphysical and macrophysical composition of cirrus in terms of ice crystal size, ice crystal shape and Ice Water Content (IWC). The IWC is an important macrophysical variable in radiative transfer (see, for example, Foot, 1988; Francis et al., 1994; Mitchell, 2002) and it is defined as the mass of ice present per unit volume and has units of gm^{-3}. For a complete review of cirrus microphysical and macrophysical properties see Lynch et al. (2002).

Since cirrus occurs at high altitudes these clouds predominantly consist of nonspherical ice crystals. The sizes and shapes of these nonspherical ice crystals can vary significantly. In terms of size cirrus ice crystals can vary between less than 50 µm to several thousand micrometres and the shapes can take on many different geometric forms (Garrett et al., 2005; Connolly et al., 2004; Gallagher et al., 2004; Heymsfield and Miloshevich, 2003; Korolev et al., 2000; McFarquhar and Heymsfield, 1996). Typically the shapes of nonspherical ice crystals that appear in cirrus can range from simple hexagonal ice columns, hexagonal ice plates, single bullets, bullet-rosettes having varying numbers of branches, to complex aggregates composed of roughened and/or distorted hexagonal columns. More recent observations demonstrate that chains of aggregates consisting of plates can also exist in tropical anvil cloud (Connolly et al., 2004) and Lawson et al. (2003) also found evidence of aggregate chains in continental anvils. Interestingly, no evidence of aggregate chains was found in anvils generated by maritime convection as reported by Lawson et al. (2003). It is remarked by Connolly et al. (2004) that the aggregate chains observed by them are strikingly similar to aggregate chains found in the laboratory under the influence of electric fields (Wahab, 1974; Saunders and Wahab, 1975).

Typical examples of ice crystal ensembles of varying shapes and sizes that might exist in cirrus are shown as a function of height in Fig. 2.1 and Fig. 2.2 (the images were provided by Andrew Heymsfield). The images shown in both figures were obtained using the Cloud Particle Imager (CPI) instrument and the CPI is described in the paper by Lawson et al. (2001). The crystal sizes shown in Fig. 2.1 are greater than 100 µm (Heymsfield and Miloshevich, 2003) and it is evident from the figure that there is little evidence of the more pristine shapes such as hexagonal columns or plates, the most common shapes appear to be rosettes and chains of rosettes and the rosettes appear spatial rather than compact. Although in Fig. 2.1 there does appear to be the odd hexagonal column, there is evidence of air inclusions, both in the single columns and in some branches of the rosettes. The shapes shown in Fig. 2.2 are dominated by bullet-rosettes or aggregates of rosettes for crystal sizes larger than 100 µm with again very little evidence of pristine ice crystal shapes such as hexagonal columns or hexagonal plates. The shape of ice crystals less than 100 µm in size is currently unknown due to the limiting resolving power of the CPI. As shown in Fig. 2.2 these shapes of less than 100 µm in size can appear as quasi-spherical or spheroidal but nonetheless may still be irregular. It is very important to characterize the size and shapes of ice crystals smaller than 100 µm as these may exist in significant concentrations and can have a large impact on the radiative properties of cirrus (Ivanova et al., 2001; Yang et al., 2001). Since ice crystals less than 100 µm in size appear 'quasi-spherical' it is often the case that such crystals are modelled as spheres as suggested by McFarquhar et al. (1999) or Chebyshev polynomials (McFarquhar et al., 2002), spheroids were suggested by Asano and Sato (1980).

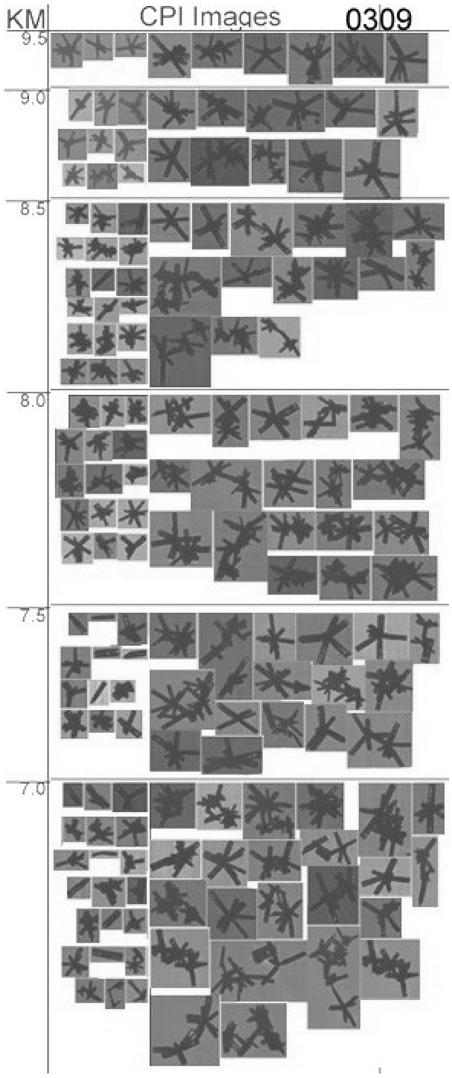

Fig. 2.1. A set of ice crystal images shown as a function of height. The images were obtained using the CPI instrument (courtesy A. Heymsfield).

Other possibilities are the Gaussian random sphere as suggested by Nousiainen and McFarquhar (2004) or droxtals as proposed by Yang et al. (2003). Although it is not currently possible to say which of these representations truly represents ice crystals less than 100 µm in size, it is, however, likely that small ice crystals are faceted as commented by Heymsfield and Platt (1984). In order to distinguish the shapes of small ice crystals an enhanced CPI is required or a new approach. A new approach could be based on two-dimensional scattering patterns as proposed by Clarke et al. (2006). In the paper by Clarke et al. (2006) it is shown that

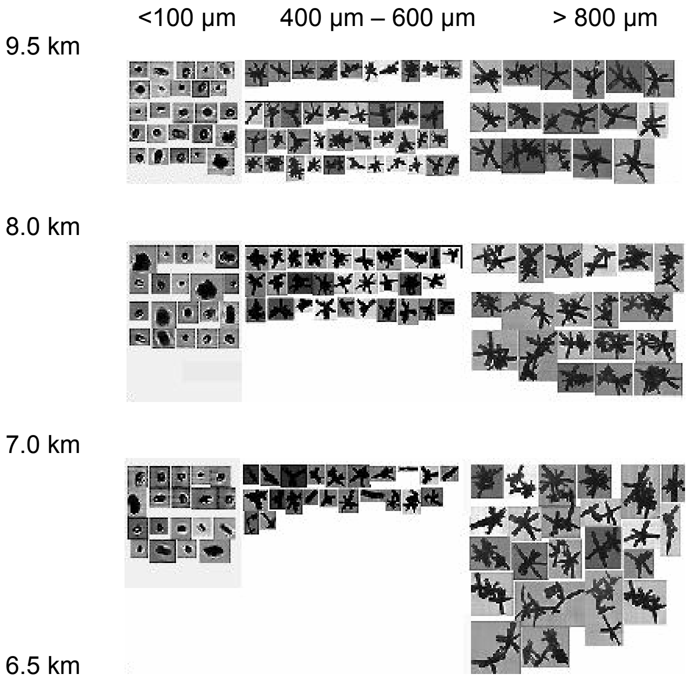

Fig. 2.2. Same as Fig. 2.1 but ice crystal size is shown on the top along the x-axis (courtesy A. Heymsfield).

the 2D scattering patterns between a small hexagonal column, hexagonal plate, rosette and droxtal are quite different and these differences could be used to potentially classify ice crystal shapes less than 100 µm in size.

From the currently available evidence it can be said that the most common type of ice crystal that inhabits synoptically generated cirrus is bullet-rosettes whilst anvil cirrus is chiefly populated by non-symmetric irregulars. This is further supported by observations made by Korolev et al. (2000) in the mid-latitudes and McFarquhar and Heymsfield (1996) whom made measurements of ice crystal size and shape in deep tropical convection.

With such a variability of ice crystal size and shape, adequately modelling and computing cirrus scattering and absorption properties is problematic; but this problem must be addressed if the net radiative impact of cirrus is to be quantified. The rest of this chapter will be devoted to reviewing the current modelling approaches to representing cirrus ice crystal shapes and the current methodologies adopted in computing their scattering and absorption properties. The chapter ends by reviewing how such ice crystal scattering and absorption properties can be tested by remotely sensing, cirrus using both airborne and space-based instruments. The chapter attempts to bring together the importance of cirrus microphysical and macrophysical properties to the light scattering problem and how these two equally important components can be combined to improve understanding of the net radiative impact of cirrus.

2.2 Cirrus ice crystal models

As can be seen from Fig. 2.1 and Fig. 2.2 the shapes of cirrus ice crystals are complex and so, in order to model their scattering and absorption properties, idealized geometric shapes are sought. The typical range of ice crystal models currently used is shown in Fig. 2.3. The modelling of shapes which have symmetric properties such as the hexagonal column, hexagonal plate and bullet-rosette is straightforward since these have a well defined three-dimensional geometry as shown in Figs. 2.3 (b), 2.3 (c), and 2.3 (d), respectively. However, as the complexity of ice crystal shape increases then there are a number of possibilities as

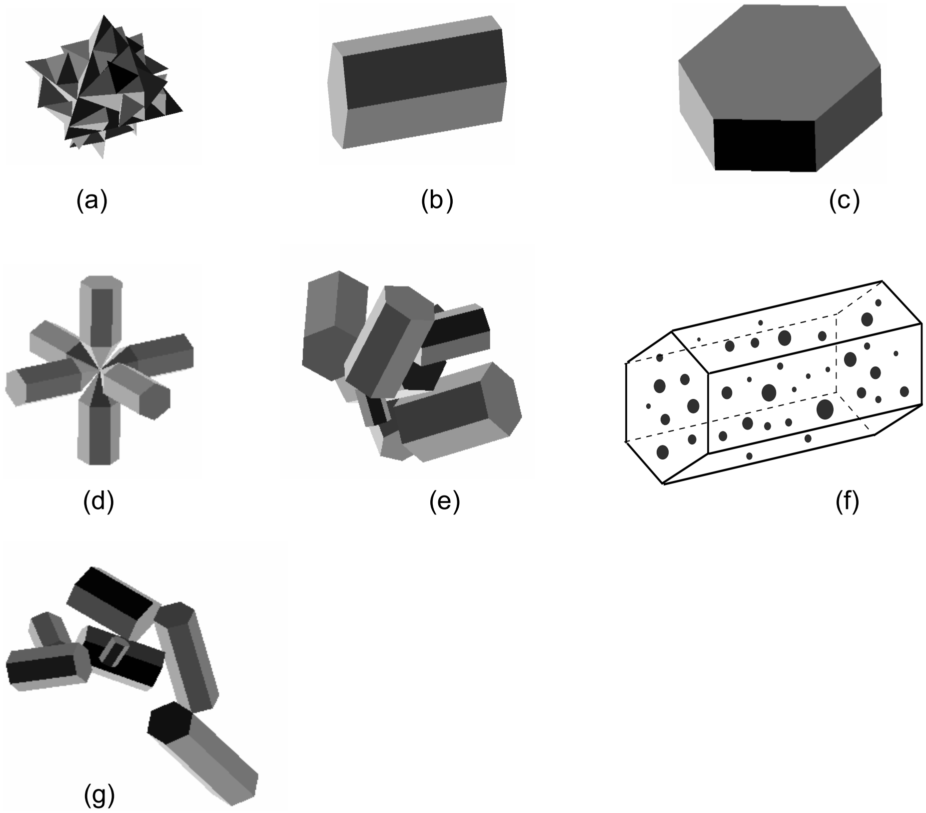

Fig. 2.3. Geometrical realizations of ice crystal shapes showing (a) randomized polycrystal, (b) pristine hexagonal ice column, (c) hexagonal ice plate, (d) six-branched bullet-rosette, (e) randomized hexagonal ice aggregate, (f) inhomogeneous hexagonal monocrystal, (g) chain-like aggregate.

to how to represent such a complexity. In Fig. 2.3 four such realizations of complex ice crystals are illustrated. In Fig.2.3 (a) the 'polycrystal' due to Macke et al. (1996) is a randomization of the second-generation triadic Koch fractal, the basic element of which is the tetrahedron and the polycrystal remains invariant with respect to size. The polycrystal is supposed to represent in one ice crystal model the variability of shape observed in Fig. 2.1 and Fig. 2.2. Figure 2.3 (e) illustrates the hexagonal ice aggregate introduced by Yang and Liou (1998); the aggregate is composed of eight hexagonal elements, the surfaces of which can be roughened. The hexagonal ice aggregate also remains invariant with respect to size. Figure 2.3 (f) shows the Inhomogeneous Hexagonal Monocrystal (IHM), which was introduced by Labonnote et al. (2001) in order to retain the simplicity of the hexagonal column but introducing randomization of the ice crystal by adding inclusions such as air bubbles and aerosol. Figure 2.3 (g) shows the chain-like aggregate introduced by Baran and Labonnote (2006) based on the Yang and Liou (1998) aggregate but with two of the original hexagonal elements elongated and re-transformed into a chain. This model is supposed to capture the more spatial and chain-like properties shown in Fig. 2.1 and Fig. 2.2.

The common feature of the polycrystal and hexagonal ice aggregate is that their aspect ratio remains invariant with respect to size. Rather than arbitrarily constructing some ice crystal model it would be desirable to predict resulting crystal shapes from an initial monomer crystal, which is allowed to aggregate. This approach has been applied by Westbrook et al. (2004), where a distribution of monomer ice crystals such as single six-branched rosettes are allowed to collide until a distribution of aggregates is produced. An example of such a fully grown ice aggregate is shown in Fig. 2.4. As can be seen from the figure the resulting aggregate has an aspect ratio greater than unity and is also spatial. These are the two properties which are common to Fig. 2.1 and Fig. 2.2. It has also been demonstrated by Westbrook et al. (2004) that the resulting aspect ratio of the ice aggregate asymptotes to 1.54 and is independent of assumptions regarding the initial monomer.

The geometric ice crystal representations illustrated by Fig. 2.3 are single model realizations but, as shown in Fig. 2.1 and Fig. 2.2, in reality ensembles of different shapes occur which Westbrook et al. (2004) attempt to emulate. It is becoming more common to construct ensembles of geometric shapes rather than assume one single geometric shape over the entire particle size distribution function. Such an approach has been utilized by Rolland et al. (2000) and McFarquhar et al. (1999, 2002). More recently, Baum et al. (2005) have demonstrated that a mixture of shapes can better represent the bulk IWC than single shape models such as the hexagonal ice aggregate. The mixture of ice crystal shapes proposed by Baum et al. (2005) comprise droxtals, hexagonal plates, solid hexagonal columns, hollow columns, bullet-rosettes and aggregates.

In this chapter another approach to representing the distribution of cirrus ice crystal size and shape by some distribution of idealized shapes is presented and has been described in Baran (2006). As Fig. 2.1 and Fig. 2.2 illustrate, ice crystal shape appears to become more progressively spatial and complex lower in the cloud. In order to mimic this change in shape as a function of crystal

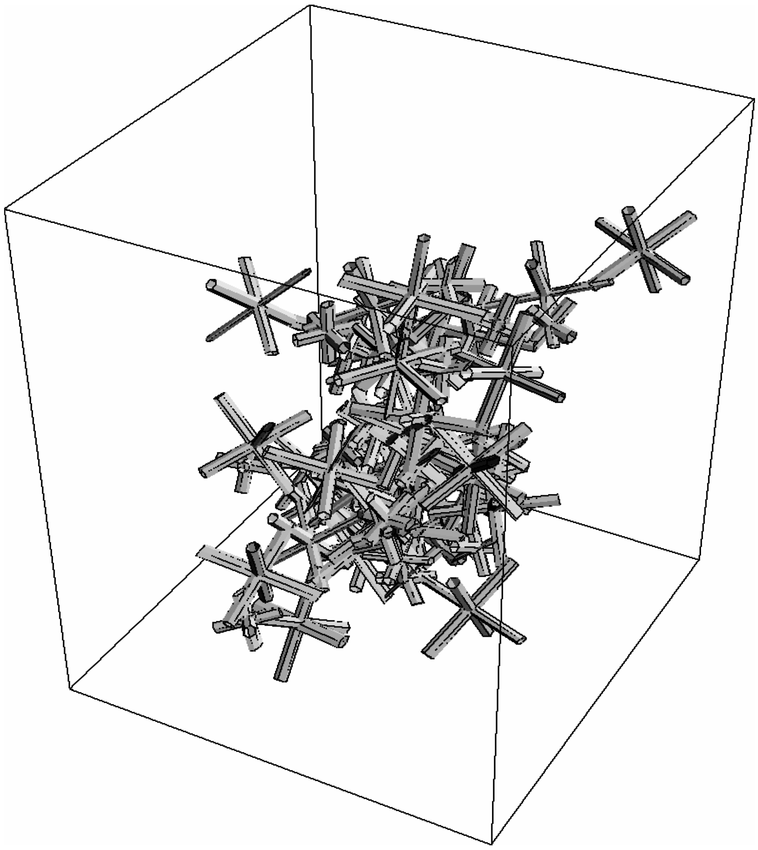

Fig. 2.4. A realization of an ice aggregate ice crystal grown from an initial six-branched hexagonal rosette. The aspect ratio of the fully grown aggregate is 1.54 (reproduced, with permission, from Baran, 2003a).

maximum dimension (literally the largest extent of the crystal) an ensemble model, as illustrated in Fig. 2.5, has been constructed. The smallest ice crystals consist of solid hexagonal ice columns assuming an aspect ratio of unity (i.e., ratio between column length and diameter). As the maximum dimension of ice crystals increase, the shapes become progressively more complex and spatial by arbitrarily attaching other column elements. One important aspect of the ensemble model shown in Fig. 2.5 is that the overall aspect ratio does not remain invariant with respect to the ice crystal maximum dimension. The various shapes in Fig. 2.5 are assumed to be distributed equally throughout the particle size distribution function. In the paper by Baum et al. (2005) the particle size distribution functions are obtained from many different field campaigns with no clear relationship between IWC and the cloud temperature (T_{c}). It would be desirable to relate the particle size distribution function (PSD) to macroscopic variables such as IWC and T_{c} such that the PSD can be generated from any given val-

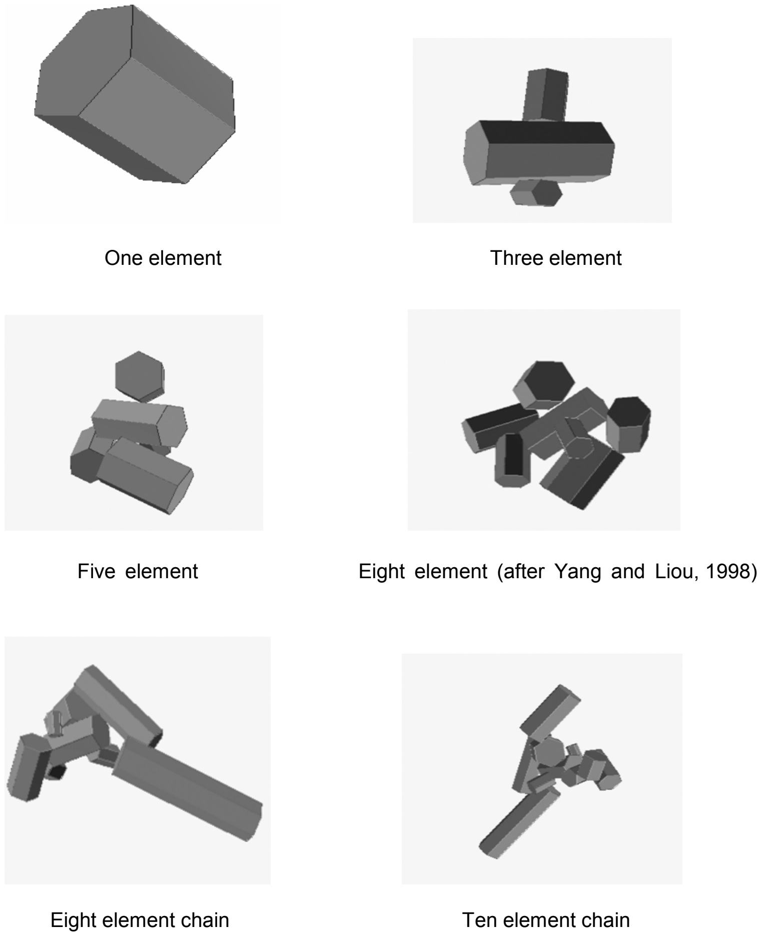

Fig. 2.5. The ensemble model. The one element model represents the smallest ice crystals taken to be a hexagonal ice column assuming an aspect ratio of unity, whilst the ten element model represents the largest ice crystals. All elements are assumed to be equally distributed in the particle size distribution function.

ues of these two variables. Such a parametrization has been realised by Field et al. (2005) and the parametrization should be of value in climate and numerical weather prediction models where IWC and T_c are important variables. The parametrization due to Field et al. (2005) is based on many *in situ* measured PSD obtained in mid-latitude stratiform ice cloud at temperatures between 0°C and −60°C. The paper demonstrates importantly that the many PSD may be represented by a single underlying PSD from which the initial PSD can be retrieved from knowledge of two moments. Field et al. (2005) make use of the IWC (second moment of the PSD) and by using T_c they obtain power laws to link IWC to any moment. However, the paper by Field et al. (2005) does not quan-

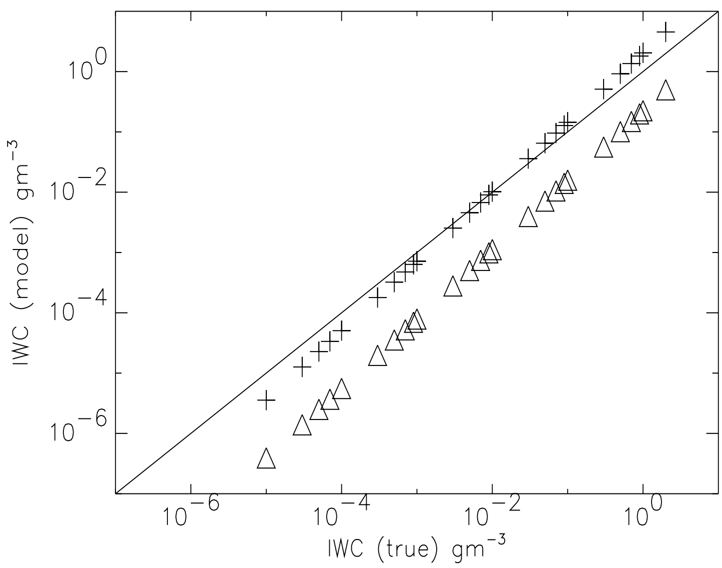

Fig. 2.6. The predicted IWC assuming the ensemble model (plus signs) and the hexagonal ice aggregate (triangles) plotted as a function of true IWC for $T_c = -30°C$. The full line shows the one-to-one relationship.

tify the contribution of ice crystals smaller than 100 µm to the PSD; however, the parametrization is independent of ice crystal shape assumptions. Therefore, from given values of IWC and T_c the PSD can be generated. From the generated PSD using the parametrization due to Field et al. (2005) the IWC can then be predicted from the ensemble model shown in Fig. 2.5. The predicted IWC from the ensemble model can then be compared with the true IWC used to generate the PSD. The results of comparing the predicted IWC from the ensemble model with the true IWC are shown in Fig. 2.6 for $T_c = -30°C$, also shown in the figure are the results for the hexagonal ice aggregate. The figure shows that the hexagonal ice aggregate is not a good predictor of the true IWC, which is consistent with Baum et al. (2005). In contrast, the ensemble model prediction of the true IWC is good. In general the ensemble model prediction of the true IWC is generally well within a factor 2. Results of comparison assuming $T_c = -60°C$ are shown in Fig. 2.7. In this case the hexagonal ice aggregate under-predicts the true IWC by significant factors whilst the ensemble model under predicts by about a factor 2 though this improves with increasing true IWC. Typical ranges of measured IWC at $T_c = -30°C$ and $-60°C$ are 0.01–1.0 gm^{-3} and 0.001–0.1 gm^{-3}, respectively (see Fig. 2.2 in Field et al., 2005, top scale). Considering the measured range of IWC, the ensemble model prediction of IWC at $T_c = -30°C$ is in excellent agreement with the true IWC and at $T_c = -60°C$ the agreement is satisfactory. It should be remarked that the measurements made by Field et al. (2005) at temperatures of $-60°C$ were at the limits of instrumental capability and the contribution of ice crystals less than 100 µm in size was

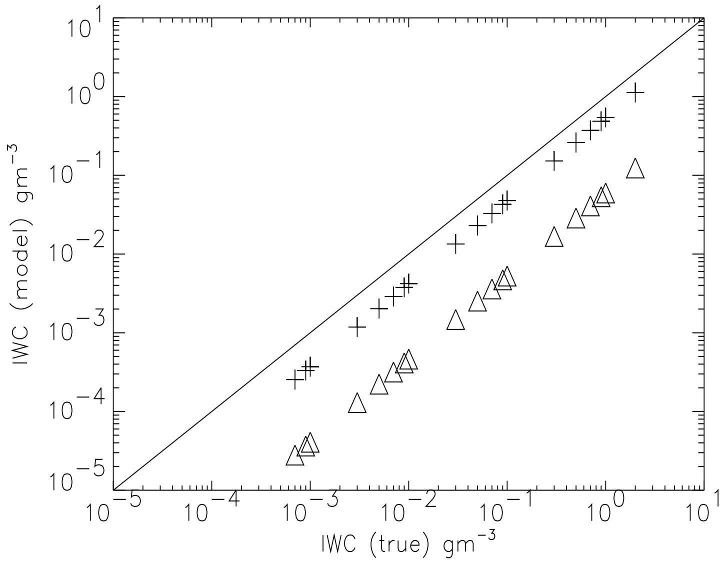

Fig. 2.7. Same as Fig. 2.6 but for $T_{\mathrm{c}} = -60°\mathrm{C}$.

ignored. Figure 2.6 and Fig. 2.7 demonstrate that it is possible to construct an ensemble ice crystal model which from the PSD predicts reasonable values for the IWC. Linking the ice crystal model to important variables such as IWC and T_{c}, via the PSD, is important if cirrus parametrization in climate models is to be further improved. Given an ensemble ice crystal model such as that shown in Fig. 2.5 the question of computing its scattering and absorption properties arise. The next section reviews computational methods currently used to obtain scattering and absorption characteristics of nonspherical ice crystals.

2.3 Computational methods applied to nonspherical ice crystals

As can be seen from Fig. 2.1 and Fig. 2.2 the range of ice crystal size and shape is significant and computation of their single scattering properties is demanding. The problem is to be able to apply some computational method to a tractable geometry resulting in stable and convergent solutions which represent the scattering and absorption properties of real ice crystals. The basic description of incident light being scattered from a collection of randomly oriented ice crystals suspended in the Earth's atmosphere is briefly outlined below.

Assuming an incident unpolarized beam of light upon an ensemble of randomly oriented ice crystals which each posses a plane of symmetry, the Stokes vector of the incident light (I_{inc}, Q_{inc}, U_{inc}, V_{inc}) is linearly related to the Stokes vector of the scattered light (I_{sca}, Q_{sca}, U_{sca}, V_{sca}) by a 4×4 scattering matrix, for each scattering angle, θ, given by (van de Hulst, 1957):

$$\begin{pmatrix} I_{\text{sca}} \\ Q_{\text{sca}} \\ U_{\text{sca}} \\ V_{\text{sca}} \end{pmatrix} = \frac{c_{\text{sca}}}{4\pi r^2} \begin{pmatrix} P_{11} & P_{12} & 0 & 0 \\ P_{21} & P_{22} & 0 & 0 \\ 0 & 0 & P_{33} & P_{34} \\ 0 & 0 & P_{43} & P_{44} \end{pmatrix} \begin{pmatrix} I_{\text{inc}} \\ Q_{\text{inc}} \\ U_{\text{inc}} \\ V_{\text{inc}} \end{pmatrix} \tag{2.1}$$

where in Eq. (2.1) C_{sca} is the ice crystal scattering cross-section (extinction efficiency multiplied by the ice crystal geometric cross-section) and r is the distance of the scattering particle from some observer. The 4×4 matrix shown in Eq. (2.1) is called the phase matrix. Due to the assumed symmetry properties of the system then, out of the eight elements shown in Eq. (2.1) only six are independent due to $P_{21} = P_{12}$ and $P_{43} = -P_{34}$ (see van de Hulst, 1957). Since incident unpolarized light has been assumed (which is the case for incident sunlight) the first element in Eq. (2.1) is proportional to the scattered light and P_{11} is called the scattering phase function. It is normalized as follows:

$$\frac{1}{2} \int_{-1}^{1} P_{11}(\theta) \sin\theta \, \mathrm{d}\theta = 1 \tag{2.2}$$

Moreover, $-P_{12}/P_{11}$ describes the degree of linear polarization (DLP). The P_{11} element and DLP are useful quantities in the remote sensing of cirrus since P_{11} and DLP depend on the shape and size of ice crystals.

In this chapter the orientation of ice crystals is assumed to be random. This assumption leads to the following question. What is the current evidence that atmospheric ice crystals are randomly oriented in space? In the paper by Chepfer et al. (1999) it was reported that at least 40% of their space-based measurements of cirrus suggested that the ice crystals were horizontally oriented. However, in more recent papers by Bréon and Dubrulle (2004) and Noel and Chepfer (2004) they conclude that the actual fraction of horizontally oriented ice crystals is more likely to be about 10^{-2}. Therefore, given this information the assumption of randomly oriented ice crystals can be generally applied, at least for solar and infrared measurements of cirrus.

In terms of radiative transfer the single scattering properties that are required to compute the radiative properties of cirrus are the volume extinction coefficient, K_{ext}, volume scattering coefficient, K_{sca}, the single scattering albedo (the ratio of the scattered energy to the total amount of attenuated energy), ω_0, and the asymmetry parameter, g. The volume extinction/scattering coefficient is defined as

$$K_{\text{ext,sca}} = \int Q_{\text{ext,sca}}(\boldsymbol{q}) \, \langle S(\boldsymbol{q}) \rangle \, n(\boldsymbol{q}) \, \mathrm{d}\boldsymbol{q} \tag{2.3}$$

where $Q_{\text{ext,sca}}(\boldsymbol{q})$ is the extinction/scattering efficiency factor (defined as the ratio between the scattering/extinction cross-section and geometric area of the ice crystal), $\langle S(\boldsymbol{q}) \rangle$ is the orientation averaged geometric area and $n(\boldsymbol{q})$ is the PSD. Each term in Eq. (2.3) is expressed as a function of the vector parameter, $\boldsymbol{q}$, which characterizes the shape and size of ice crystal. The single scattering albedo is given by

$$\omega_0 = K_{\text{sca}}/K_{\text{ext}} \tag{2.4}$$

and the asymmetry parameter is a parametrization of the P_{11} element into a single number which describes how much incident radiation is scattered into the backward and forward hemispheres and can take on values between -1 and 1 depending on the size, shape, and refractive index of the scatterer. The formal definition of g is the average cosine of the scattering angle:

$$g = \langle \cos\theta \rangle = \int_{-1}^{1} \mathrm{d}(\cos\theta) P_{11}(\cos\theta)\cos\theta\,. \tag{2.5}$$

In order to compute or measure g from Eq. (2.5) the angular dependence of the P_{11} element must be known. The asymmetry parameter is a very important quantity in climate models as choice of g determines the radiative impact of cirrus (Stephens et al., 1990). The reason why choice of g is so important is because the backward reflection of incident sunlight assuming conservative scattering depends on $1 - g$, so for small and large values of g reflection of sunlight back to space increases and decreases, respectively. It is, therefore, necessary to constrain the value of g so that the most representative value can be applied to climate models. Calculations of g for the various ice crystal models described in section 2.2 range from 0.74 for the polycrystal (Macke et al., 1996), 0.77 for the hexagonal ice aggregate (Yang and Liou, 1998) and 0.75–0.84 for the solid hexagonal column (Takano and Liou, 1989a). It is possible to 'measure' g using the Cloud Integrating Nephelometer (CIN) described in Gerber et al. (2000). The P_{11} element measured by CIN is truncated at a scattering angle of 10°, thus the full phase function is not utilized in the 'measurement' of g. The CIN instrument has measured g in an Arctic ice cloud consisting of bullet-rosettes at visible wavelengths, suggesting values around 0.74. In tropical cirrus CIN measured g values of 0.75 ± 0.01 as reported in Garrett et al. (2003). In tropical anvil cloud CIN generally measured g values ranging between 0.70 and 0.74 as discussed in Garrett et al. (2005). Baran et al. (2005) estimated the asymmetry parameter using ground-based Polar Nephelometer measurements of Antarctic ice crystals as they fell into a light scattering chamber, and the irregular ice crystal ensemble was found to have a g value of 0.74 ± 0.02. In the paper by Field et al. (2003) the asymmetry parameter in mid-latitude cirrus was estimated to be 0.76 using an airborne light scattering probe by fitting a phase function to the angular intensity measurements that depends on g only. Currently, there appears to be some convergence of measured g values of around 0.74 ± 0.02 for atmospheric ice crystals according to the literature. However, further measurements of g are required both in the laboratory of actual ice crystals and in the field using new instrumentation that captures a near-complete phase function before one can say that true convergence has been achieved.

The computation of Eqs (2.1)–(2.5) over the entire spectrum of ice crystal size is not an easy task since typical cirrus ice crystal size parameters (product of particle characteristic size and wavenumber, where the wavenumber is $2\pi/\lambda$ and λ is the incident wavelength) can range between less than unity to thousands. Currently, there is no one single computational method that is capable of covering the whole cirrus size parameter space. As a result approximate methods are still required to bridge the gap between small size parameters, intermediate size parameters and large size parameters.

Electromagnetic methods are usually applied to ice crystals covering small size parameter space of less than about 40. The Finite-Difference-Time-Domain (FDTD) method has been applied to compute the single scattering properties of the hexagonal ice aggregate up to a size parameter of about 20 (Yang and Liou, 1995; Yang et al., 2000, 2004) and Havemann et al. (2003) have applied the T-matrix method to the solid finite hexagonal ice column at size parameters of up to about 40. Sun et al. (1999) have applied the FDTD method to the ice sphere at size parameters of up to 40. The accuracy of the FDTD method has been tested by Baran et al. (2001a) against the T-matrix method for a finite randomly oriented solid hexagonal ice column and it was found that the relative errors for C_{ext}, ω_0, and g were less than 1%. The FDTD method has also been applied to more general shapes such as the bullet-rosette (Baum et al., 2000), Gaussian random particles (Sun et al., 2003) and droxtals (Yang et al., 2003). The T-matrix method has now been applied to more general polyhedral prisms by Kahnert et al. (2001). Other electromagnetic methods that have been applied to ice crystals include the Separation of Variables Method (SVM) developed by Rother et al. (2001) to compute the scattering matrix elements of the infinite hexagonal ice column. Kokhanovsky (2005a,b, 2006) has used the discrete dipole approximation (DDA) to compute the scattering properties of hexagonal and cubic ice crystals. By combining desirable properties of the T-matrix and DDA, Mackowski (2002) has developed the Discrete Dipole Method of Moments (DDMM) approach, which shows promise for computing the single scattering properties of ice crystals for size parameters of about 40. The boundary-element method has been successfully applied by Mano (2000) to compute the single scattering properties of oriented finite hexagonal ice columns for size parameters of 50. An extensive review of electromagnetic methods can be found in Mishchenko et al. (2002) and Kahnert (2003).

For the intermediate size parameter range ($\sim$20 to 60), there are a number of physical optics based approaches which fill the gap between 'exact' and approximate methods. In the paper by Yang and Liou (1996) it is shown that the method of Improved Geometric Optics (IGO) applied to the geometry of the solid hexagonal ice column converges to FDTD solutions for the extinction cross-section and single scattering albedo at size parameters around $\sim$20. This holds for the P_{11} element in Eq. (2.1) as well (Yang and Liou, 1995). The physical optics approach of Muinonen (1989) could also be applied to ice crystals. More recently, a computationally fast edge diffraction method has been proposed by Hesse and Ulanowski (2003) and further developed in Clarke et al. (2006). This new approach has been specifically developed for ice crystals with facets, though in principle it could be applied to any arbitrary dielectric faceted object. Diffraction on facets has been compared with SVM in computing the P_{11} element and the asymmetry parameter, assuming oriented hexagonal columns of size parameters 50 and 100 (Hesse et al., 2003). Borovoi and Grishin (2003) have developed a proper ray-tracing method for computation of the Jones scattering matrix inclusive of diffraction and phase information is accounted for exactly, which has been applied to compute the backscattering properties of large hexagonal ice columns. For size parameters much larger than 60, then ray-tracing can be applied to any arbitrary ice crystal shape. The first solution of the 3D problem assuming hexagonal columns was achieved by Wendling et al. (1979) but without polarization. Polarization was incorportated by Cai and Liou (1982) and further refinements such as including birefringence and particular ice crystal orientations were reported in Takano and Liou (1989a,b). The ray-tracing method was applied to more complex shapes most notably by Macke (1993) and Macke et al. (1996) in which it was shown for the first time that the polycrystal could produce asymmetry parameters as low as 0.74 at non-absorbing wavelengths. Borovoi et al. (2000) computed the backscattering cross-section of arbitrarily oriented hexagonal ice columns at visible wavelengths using ray-tracing. It was found that for a tilt angle of 32.5° a very large backscattered intensity peak occurs, which is explained by a corner-reflector effect. The authors suggest that this finding could be used to discriminate between aligned hexagonal ice plates and hexagonal ice columns by using slant lidar. More recently, Borovoi et al. (2005) proposed an optical model for cirrus clouds by parametrizing the phase functions for a variety of randomly oriented ice crystal particles by means of weight coefficients for the wedges occurring in each ice crystal shape.

Other methods that have been suggested to compute the single scattering properties of nonspherical ice crystals are modified anomalous diffraction theory proposed by Mitchell et al. (1996), which has been further developed in Mitchell (2002) and Mitchell et al. (2006). The modified anomalous diffraction theory is based on the Bryant and Latimer (1969) approximation (BL), which approximates the original van de Hulst (1957) anomalous diffraction theory (ADT). The original ADT assumes that the size of particle is much greater than the incident wavelength and that the refractive index is close to unity. The BL approach attempts to apply ADT to nonspherical particles by taking the ratio of the particle volume-to-averaged cross-sectional area as a size and phase shift parameter. The original ADT and the BL approximation do not incorporate internal reflection, surface waves or large angle diffraction. The approach of Mitchell et al. (1996) was to incorporate this missing physics into the BL approximation. However, Sun and Fu (2001) compared the Bryant and Latimer approximation against exact ADT for computing the extinction coefficient of the finite hexagonal column and showed that BL could be in significant error. Though Mitchell et al. (2001, 2006) showed that modified ADT was in good agreement with laboratory-based experiments of hexagonal column ice crystal extinction efficiency between the wavelengths of 2.2 and 16.0 μm. Since ADT has no angle dependence (except at $\theta \to 0°$) then neither the P_{11} element at arbitrary θ nor the asymmetry parameter can be calculated.

The application of the electromagnetic methods to the geometries outlined in section 2.2 is a complex task. Therefore, Baran (2003b) proposed that it might be possible to simulate the infrared properties of more complex ice crystals by representing the complex ensemble by some ensemble of symmetric ice crystals of varying aspect ratio. In the paper by Baran (2003b) the T-matrix method due to Mishchenko and Travis (1998) was applied to an ensemble of circular ice cylinders and by conserving the volume-to-projected area ratio of the hexagonal ice aggregate it was shown that the total optical properties (C_{ext}, ω_0 and g) of the more complex shape could be simulated to well within 4% when compared against solutions from FDTD. The method in principle could be applied to any ice crystal shape at infrared wavelengths and, since C_{ext} and ω_0 depend largely on the volume-to-area ratio, it is expected to work well for those quantities. Similar approaches of representing scattering from ensembles of complex non-symmetric shapes by ensembles of more symmetric shapes have also been applied to scattering by aerosols (Kahnert et al., 2002a). The difficulty with using ensembles of simpler shapes to represent scattering from more complex shapes is that angle-dependent quantities such as the matrix elements in Eq. (2.1) are more difficult to simulate as demonstrated by Kahnert et al. (2002b). It was shown by Lee et al. (2003) that randomly oriented finite circular cylinders could be used to simulate the single scattering properties of randomly oriented hexagonal ice columns at infrared wavelengths to within a few percent.

To bridge the gap between small and large size parameter space Liou et al. (2000) proposed the 'unified' method where FDTD and IGO are combined to calculate the single scattering properties over the whole ice crystal PSD, and in principle this method can be applied to any ice crystal shape. The approach proposed by Fu et al. (1999) is similar to the 'unified' method.

The methods outlined in this section can be used to compute the single scattering properties of the ice crystal realizations outlined in section 2.2. However, the problem in computing the radiative properties of cirrus with such a diversity of ice crystal shape is how best to represent the single scattering properties by some single dimension? Should that dimension be maximum size, chord length, or facet length? What is required is a common dimension such that the radiative properties can be computed independently of ice crystal shape and shape of the PSD. For example, water clouds are more straightforward (Slingo, 1989) since these are composed of water spheres and their PSDs are not as dispersed as cirrus. In recent years there appears to have been a consensus of opinion as to which dimension to apply in computing the radiative properties of cirrus. Initially, it was proposed by Foot (1988) that cirrus radiative properties might well be represented if the distribution of ice crystal shapes and sizes was expressed as a ratio of the distribution volume-to-distribution averaged cross-section. This proposition of an effective dimension has now been adopted by a number of authors when computing cirrus solar bulk single scattering properties or retrieving cirrus microphysical/macrophysical properties (Francis et al., 1994; Fu, 1996; Yang et al., 1997; McFarquhar and Heymsfield, 1998; Wyser and Yang, 1998; Mitchell, 2002; McFarquhar et al., 2002; Baran et al., 2003; Baran and Havemann, 2004). Thus throughout the rest of this chapter the cirrus PSD is characterized by an effective dimension called the effective diameter, D_{e}, defined as,

$$D_{\text{e}} = 3/2 \int V(D_{\text{m}}) n(D_{\text{m}})\, \mathrm{d}D_{\text{m}} \Big/ \int \langle S(D_{\text{m}}) \rangle\, n(D_{\text{m}})\, \mathrm{d}D_{\text{m}} \tag{2.6}$$

where $V(D_\mathrm{m})$ is the geometric volume of the ice crystal and $\langle S(D_\mathrm{m})\rangle$ is the orientationally averaged geometrical cross-section of ice crystals in a unit volume of a cloud. For monodisperse spheres, D_e equates to their diameters.

It follows for large convex ice crystals in random orientation (Kokhanovsky, 2004),

$$K_\mathrm{ext} = 3f/D_\mathrm{e} \qquad 2.6\mathrm{a}$$

where $f = IWC/\rho$ is the volumetric concentration of ice crystals, ρ is the density of ice. This confirms that Eq. (2.6) is a useful parameter to characterize size/shape distributions with respect to calculations of light extinction in cirrus. How universal is Eq. (2.6a) for calculations of K_ext? Can this concept be applied at all wavelengths? In the papers by Mitchell (2002) and Baran (2005) it is shown that the concept breaks down at infrared wavelengths. This is demonstrated in Fig. 2.8 where the mass extinction coefficient (K_ext/IWC) for 30 PSDs is plotted as a function of D_e for six wavelengths in the infrared. The figure from Baran (2005) shows that the mass extinction coefficient for the shorter wavelengths is still inversely proportional to D_e as given by Eq. (2.6a), but as the wavelength increases this relationship begins to break down. At wavelengths between 20 µm to 30 µm the concept outlined above (see Eqs. (2.6) and (2.6a)) cannot be generally applied to compute the radiative properties of cirrus. Eq. (2.6a) only has physical meaning when the ice crystal size is much larger than the incident wavelength; this is not surprising since it is fundamentally based on the principle of geometric optics. It should be pointed out here that the simple optical parameter – effective diameter relationship does not hold for the asymmetry parameter since this fundamentally depends on the shape of ice crystals as demonstrated by Kokhanovsky and Macke (1997) and Wyser and Yang (1998).

Given the geometric ice crystal realizations described in section 2.2 and the means to compute their single scattering properties the next section describes how these ice crystal models are tested using remote sensing.

2.4 Airborne and satellite remote sensing of cirrus at solar and infrared wavelengths

As pointed out in section 2.3 the two most useful quantities to use from Eq. (2.1) in the remote sensing of cirrus are the phase function and the degree of linear polarization. Calculations of the phase function and the ratio P_{12}/P_{11} are shown in Fig. 2.9 and Fig. 2.10, respectively. The calculations assume a bullet-rosette (Fig. 2.3 (d)) and a distorted bullet-rosette each having a maximum dimension of 100 µm using a complex refractive index for ice taken from Warren (1984) at the wavelength of 0.865 µm. The reason why distortion is applied in the calculations shown in Figs. 2.9 and 2.10 to the ice crystal geometry is to randomize the ice crystal such that the symmetry properties that are responsible for optical features such as halos are removed, thereby producing a featureless phase function. The method of ray-tracing due to Macke et al. (1996) was applied to the bullet-rosette geometry to calculate the scattering matrix elements. Also,

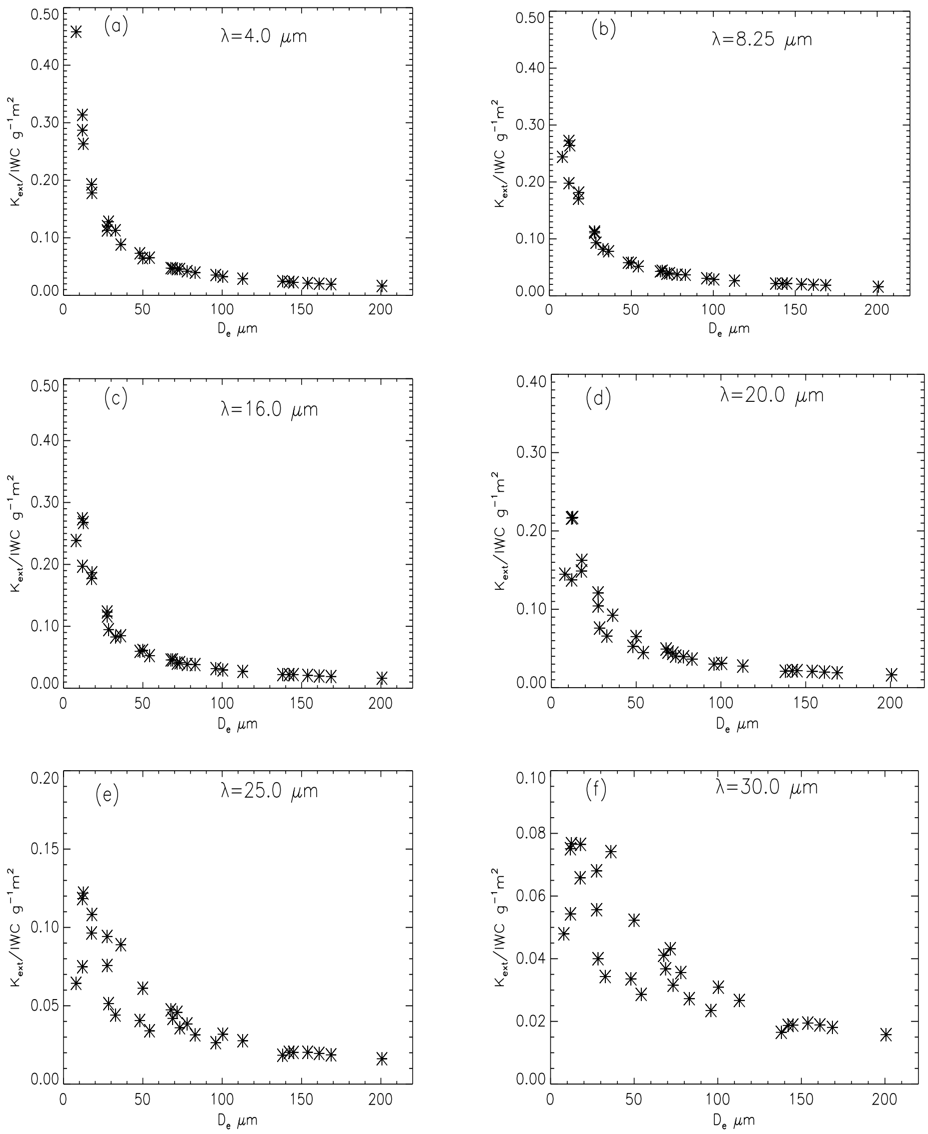

Fig. 2.8. The mass extinction coefficient, $K_{\text{ext}}/\text{IWC}$ in units of g^{-1}m^2, plotted as a function of effective diameter, D_{e}, at the wavelengths of: (a) 4.0 µm, (b) 8.25 µm, (c) 16.0 µm, (d) 20.0 µm, (e) 25.0 µm, (f) 30.0 µm. The mass extinction coefficient has been calculated using size distribution functions from Fu (1996) and Mitchell et al. (1996) (reproduced, with permission, from Baran, 2005).

shown in Fig. 2.9 for comparison is the analytic phase function due to Baran et al. (2001b). This function is defined by different expressions depending on the asymmetry parameter. In particular, it follows

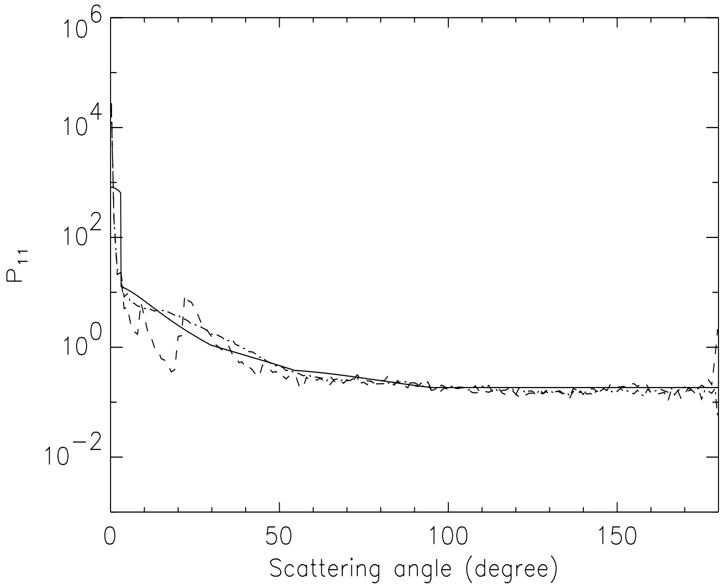

Fig. 2.9. The phase function plotted as a function of scattering angle assuming a randomly oriented six-branched bullet-rosette shown as the dashed line. The phase function of the randomized six-branch bullet-rosette is shown as the dashed-dotted line and the full line represents the analytic phase function calculated assuming an asymmetry parameter value of 0.78. The six-branched bullet-rosette is assumed to have a size of 100 µm and the incident wavelength is assumed to be 0.865 µm with an associated complex refractive index for ice of $1.304 + \mathrm{i}2.40 \times 10^{-7}$ (reproduced, with permission, from Baran and Labonnote, 2006).

$$P_{11} = \begin{cases} \dfrac{1-g^2}{(1+g^2-2g\cos\theta)^{3/2}}\alpha\cos\theta : \theta \leq 54.8^\circ \\ \dfrac{1-g^2}{(1+g^2-1.5g\cos\theta\sin\theta)^{3/2}} : \theta > 54.8^\circ \end{cases} \tag{2.7}$$

at $g < 0.7$ and

$$P_{11} = \begin{cases} \dfrac{1-g^2}{(1+g^2-2g\cos\theta)^{3/2}}\alpha\cos^{128}\theta : \theta \leq 3^\circ \\ \dfrac{1-g^2}{1+g^2-2g\cos\theta(1.3\theta)^{1.2}}\cos\theta : 3^\circ < \theta \leq 30^\circ \\ \dfrac{1-g^2}{1+g^2-2g\cos\theta(\Delta\theta)^{\sigma}}\cos\theta : 30^\circ < \theta \leq 54.8^\circ \\ \dfrac{1-g^2}{(1+g^2-1.5g\cos\theta\sin\theta)^{3/2}} : 54.8^\circ < \theta \leq 95^\circ \\ P_{11} = 95^\circ : \theta > 95^\circ \end{cases} \tag{2.8}$$

Table 2.1. Values of the coefficients A, B, C, and σ for various values of the asymmetry parameter, g

g	A	B	C	σ
$0.70 \le g \le 0.80$	148.1	202.5	49.49	0.68
$0.80 \le g \le 0.90$	277.1	510.2	232.9	0.68
$g \ge 0.90$	421.9	827.1	406.3	0.71

Table 2.2. Values of the coefficient β for various values of the asymmetry parameter, g

g	β
$g < 0.30$	1.25
$0.30 \le g < 0.45$	1.50
$0.45 \le g < 0.60$	1.23
$0.60 \le g < 0.70$	1.095

at $g \ge 0.70$; Here σ is given in Table 2.1 and

$$\Delta = \left(\frac{1-g}{4.6}\right) + g \tag{2.9}$$

The value of α is given by the following equations for the values of g shown,

$$\alpha = \begin{cases} \dfrac{\beta}{\sqrt{1-g}} & : g < 0.3 \\ \dfrac{1}{\sqrt{\beta g}} & : 0.3 \le g < 0.7 \\ \dfrac{N}{\sqrt{g}} & : g \ge 0.7 \end{cases} \tag{2.10}$$

In Eq. (2.10), N is a polynomial fit to the asymmetry parameter to ensure that P_{11} is correctly normalized to 4π, and $N = A - Bg + Cg^2$. The values for each of the coefficients A, B, C and σ for various ranges of g are given in Table 2.1 and values for β are given in Table 2.2.

This is a featureless phase function modelled on a laboratory phase function obtained from an ensemble of nonspherical ice crystals (Volkovitskiy et al., 1980, referred to as the VPP phase function); it is a linear-piecewise parametrization of the Henyey–Greenstein phase function (Henyey and Greenstein, 1941) and is entirely generated by the asymmetry parameter.

As can be seen from Figs. 2.1 and 2.2, atmospheric ice crystals are not pristine. They may be distorted or roughened, or contain inclusions. All these processes would remove or reduce any angular features present on the scattering phase function or degree of linear polarization (Macke et al., 1996; Mishchenko and Macke, 1997; Yang and Liou, 1998; Labonnote et al., 2001; Sun et al., 2004; Ulanowski et al., 2006). Fig. 2.9 shows that with no distortion the bullet-rosette

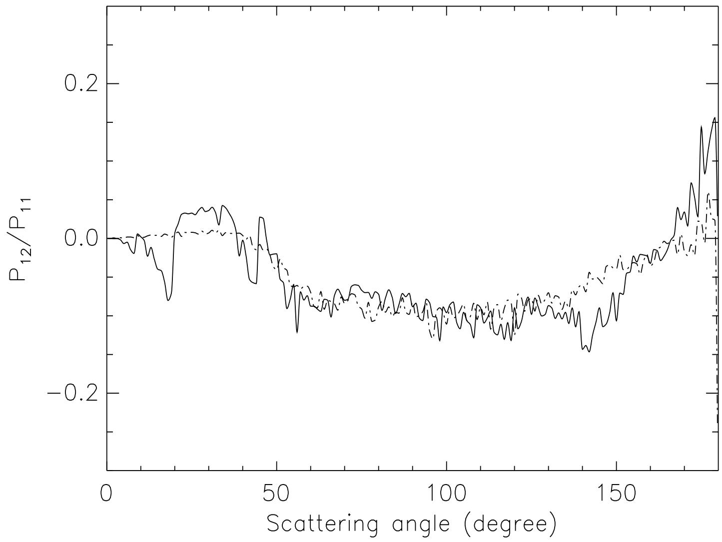

Fig. 2.10. Same as Fig. 2.9 but for the degree of linear polarization and the six-branched bullet-rosette and randomized six-branched bullet-rosette are represented by the full line and dashed-dotted line, respectively (reproduced, with permission, from Baran and Labonnote, 2006).

exhibits typical halo features present on the phase function at scattering angles of about 10°, 22°, and 42° with the 'ice bow' appearing at about 150° and retro-reflection peak at 180°. All pristine faceted ice crystals such as hexagonal columns, and hexagonal plates would also exhibit typical halos and enhanced backscattering intensities (Borovoi et al., 2000). The distorted bullet-rosette appears featureless with distinct halos and backscattering enhanced intensities removed and by a scattering angle of 50° matches the analytic phase function. The angular features present in the undistorted bullet-rosette phase function are reflected in the degree of linear polarization shown in Fig. 2.10. Therefore, Fig. 2.9 and Fig. 2.10 suggest that remote sensing instrumentation may be used to test whether cirrus is chiefly composed of pristine faceted ice crystals or more complex particle shapes. The rest of this chapter concentrates on how the idealized model geometries presented in section 2.2 and their predicted single scattering properties described in section 2.3 can be tested using aircraft and satellite data.

2.4.1 Airborne remote sensing of cirrus

To test ice crystal model predictions of the scattering phase function multi-angular radiometric measurements are required of cirrus from below and above the cloud. In the paper by Foot (1988) an airborne-based method of testing model phase functions is described where the aircraft flies in an orbit below or above the cirrus at a particular banking angle, at a distance of 1 km or several km from the cirrus base or top. With the solar zenith angle fixed, and the azimuthal angle varying, the scattered radiance from the same section of cirrus is measured as the orbit is completed, thereby describing the scattered radiance, in principle, between the scattering angles of about 5° to 180°, depending on banking angle and solar geometry. An example of measuring the phase function of cirrus using this airborne technique is shown in Fig. 2.11 from Baran et al. (2001b, Fig. 4). The figure is derived from aircraft-measured multi-angle radiance measurements obtained at the wavelength of 0.87 μm from the aircraft orbit below the cirrus on the 9th November 1995 off the north-east coast of England. The solar zenith angle at the time of the orbit was measured to be 74° and the aircraft was banked at an angle of about 53°, which enables the phase function to be sampled between the scattering angles of 21° to 127° relative to the Sun. Each set of results shown in Fig. 2.11 were offset by a factor 10 to aid clarity. The model ice crystals assumed in Fig. 2.11 are the small hexagonal ice column, small six-branched bullet-rosette, large six-branched bullet-rosette, small hexagonal ice aggregate, large hexagonal ice aggregate, the VPP and analytic phase functions. The single scattering properties for each of the ice crystal models were obtained from the method of improved geometric optics due to Yang and Liou (1996) and are listed in Table 2.3 in the form of D_e, ω_0 and g. The asymmetry parameter value assumed to generate the analytic phase function in Fig. 2.11 was 0.80 and the VPP phase function asymmetry parameter was estimated to be 0.85 by Foot (1988). The measured solar radiances were simulated using a Monte Carlo multiple-scattering model due to Kite (1987), with different values of extinction optical thickness, τ_{ext}, D_e, and solar zenith angle as input parameters. The figure shows that single model phase functions representing hexagonal ice columns, hexagonal ice plates, bullet-rosettes or the hexagonal ice aggregate do not describe the measured angular radiometric data well between the scattering angles of 20° to about 125° at the wavelength of 0.87 μm. However, phase functions such as the Volkovitskiy et al. (1980) or analytic that represent scattering from an ensemble collection of nonspherical ice crystals do represent the measured angular radiometric data well. This finding is consistent with the result found by Foot (1988) and Francis et al. (1999). The papers by Francis et al. (1999) and Baran et al. (2001b) demonstrate that phase functions,

Table 2.3. Single-ice-crystal models assuming the small hexagonal ice column (Small column), small six-branched bullet-rosette (Small bullet/rosette), large six-branched bullet-rosette (Large bullet/rosette), small hexagonal ice aggregate (Small aggregate), and large hexagonal ice aggregate (Large aggregate)

Ice crystal model	D_e (μm)	ω_0	g
Small column	9.3	1.0	0.67
Small bullet/rosette	4.0	1.0	0.73
Large bullet/rosette	79.0	1.0	0.83
Small aggregate	5.30	1.0	0.76
Large aggregate	134.0	1.0	0.77

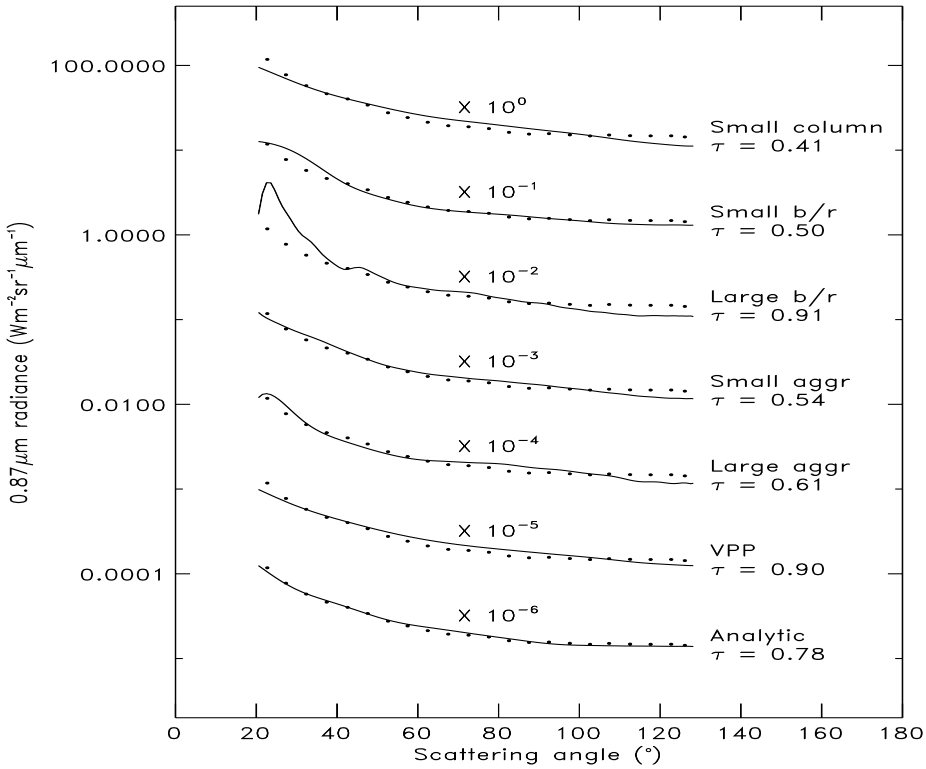

Fig. 2.11. The measured transmitted 0.87 μm radiance plotted against scattering angle with the filled circles representing the airborne radiance measurements and the full lines representing the predicted intensity assuming various ice crystal models. The model ice crystals assumed were the small hexagonal ice column, Small b/r (small bullet-rosette), Large b/r (large bullet-rosette), Small aggr (hexagonal aggregate), Large aggr (hexagonal aggregate), the Volkovitskiy et al. 1980 and analytic phase functions, respectively. The values on the right-hand side of the figure are the optimally derived optical thickness, τ, derived for each of the assumed ice crystal models. The mean experimental value found for τ was $\tau = 0.75 \pm 0.08$ (reproduced, with permission, from Baran et al., 2001).

such as the analytic, representing an ensemble of ice crystals rather than single ice crystals best represent multi-angular radiometric data obtained from below cirrus.

The infrared radiative properties of cirrus are also very important when parametrizing cirrus for climate models as demonstrated by Edwards et al. (2007). Recently, simultaneous airborne high-resolution measurements of cirrus at solar and infrared wavelengths have become available and examples of such measurements are shown in Baran and Francis (2004). In that paper the high-resolution radiometric measurements were obtained in eleven sections above a piece of semi-transparent cirrus located north of Scotland during October 2000. Since both solar and infrared measurements were made simultaneously the optical thickness above the cloud was retrieved at the wavelengths of 0.87 µm and 11.0 µm assuming hexagonal ice columns and randomized hexagonal ice aggregates. To simulate the solar and infrared high-resolution measurements and retrieve the optical thickness the radiative transfer model used was due to Edwards and Slingo (1996) assuming a plane-parallel cloud, which has been extended to radiance space by using the spherical harmonic method. This method fully takes into account the strong forward scattering peak of the ice crystal phase function (Ringer et al., 2003). The angular distribution of the radiance is decomposed into a series of spherical harmonics, with the order at which the infinite series is truncated determining the accuracy of the calculated radiance. For the radiance calculations presented in this chapter the truncation of the direct radiance has been set to 399, with the diffuse truncation being set to 21. For the infrared calculations, the diffuse truncation has been set to 19. Applying this radiative transfer model to the data the D_e (see Eq. (2.6)) values found for the hexagonal ice column that best fits both the solar and infrared high-resolution measurements were 67 µm and 87 µm. The aspect ratio of the hexagonal ice columns is based on the tabulations from Mitchell and Arnott (1994). The hexagonal ice aggregate is randomized by roughening the mantle surfaces as described in Yang and Liou (1998) and the best-fit D_e value found for this model was 78 µm. Figure 2.12 shows the retrieved optical thickness for all eleven sections assuming the two model ice crystals. In the case of the hexagonal ice column consistency in the retrieved optical thickness could not be found for all eleven sections. However, for the randomized ice aggregate consistency was found for all eleven sections. The figure demonstrates that for this case the radiative properties of the cirrus were best represented by complex randomized ice crystals. An example of high-resolution infrared measurements obtained from the optically thinnest section is shown in Fig. 2.13 (from Baran and Francis, 2004, Fig. 9c). Figure 2.13 shows brightness temperature differences between model and measurements; the dotted line shows the scene variability (i.e., the cloud was not uniform) in the high-resolution measurements. The figure shows that the cirrus radiative properties between the wavelengths of 3.3 µm and 16.0 µm are well predicted within the bounds of the scene variability for this particular case. In the case of airborne remote sensing of cirrus the generality of testing the predictions of phase functions or single scattering properties by assuming some ice crystal model is limited to relatively few cases. For this reason it is important to obtain space-based measurements of cirrus through the use of satellites, which are able to sample cirrus over many cases.

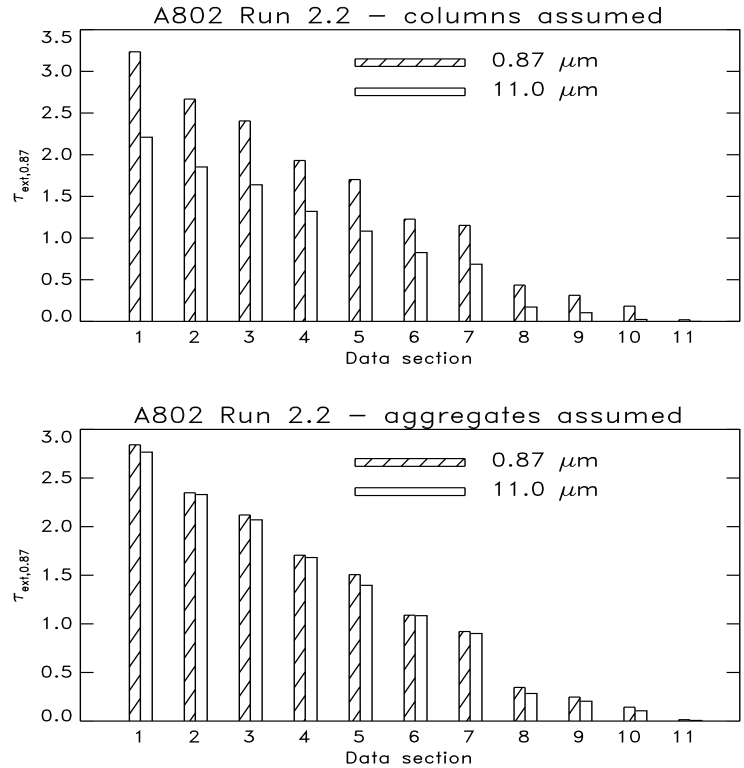

Fig. 2.12. Comparison of the best-fit optical thickness (referenced to τ_{ext} at 0.87 µm), retrieved from the airborne radiance measurements at 0.87 µm and infrared measurements at 11.0 µm, assuming (a) pristine hexagonal ice columns and (b) hexagonal ice aggregates (reproduced, with permission, from Baran and Francis, 2004).

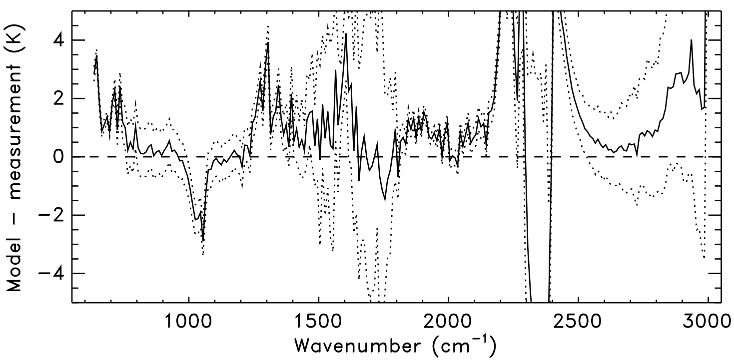

Fig. 2.13. An example of high-resolution radiometric data showing brightness temperature differences plotted against wavenumber in units of cm^{-1} ($\nu = 10000/\lambda$; so $\nu = 1000\,\text{cm}^{-1}$ corresponds to $\lambda = 10.0\,\mu\text{m}$) between simulations assuming the hexagonal ice aggregate model and the measurements. The dotted line in the figure represents the scene variability (after Baran and Francis, 2004).

2.4.2 Satellite remote sensing of cirrus

So that the single scattering properties of model ice crystals can be tested it is necessary to have space-based instruments which are able to sample the model phase function and/or polarization properties at a number of scattering angles. Currently, there are three satellites that are capable of testing model phase functions. One such instrument is the Along Track Scanning Radiometer (ATSR-2) described in Baran et al. (1999). This instrument is dual-viewing and has been used to infer ice crystal shape at non-absorbing and absorbing wavelengths (Baran et al., 1999, 2003). More recently, McFarlane et al. (2005) have made use of an instrument called the Multiangle Imaging Spectroradiometer (MISR) to infer ice crystal habit. Combining MISR with the Moderate Resolution Imaging Spectroradiometer instrument (MODIS) McFarlane et al. (2005) are able not only to estimate ice crystal shape but also to retrieve ice crystal size, since both instruments are located on the same satellite. The MISR instrument measures at solar wavelengths and has up to nine viewing angles, whilst the single-view MODIS instrument has its channels located at non-absorbing and absorbing wavelengths, which makes the retrieval of ice crystal size possible (Baum et al., 2000). The third instrument that can be utilized to study the angular reflection properties of cirrus is called the Polarization and Directionality of the Earth's Reflectances (POLDER) and a description of this instrument can be found in Buriez et al. (1997). The unique feature of POLDER is that it measures not only light reflection from cirrus but also the polarized reflectance defined as the ratio between the normalized polarized radiance and the solar zenith angle. The POLDER instrument can measure cirrus reflection function and polarization properties at up to 14 different viewing directions and can sample the phase function and the degree of linear polarization between the scattering angles from 60° to 180° dependent on latitudinal position as described in the paper by Labonnote et al. (2001). This simultaneous combination of measurements in both reflection and polarization space is very important for inferring information about the complexity of cirrus particle habits, as demonstrated by Baran and Labonnote (2006). The importance of this combination in terms of reflection is shown in Fig. 2.14 (taken from Baran and Labonnote (2006, Fig. 6), which shows the POLDER measured spherical albedo (SA) differences (i.e., measurements – model) for a variety of randomized ice crystal models plotted as a function of scattering angle. The methodology of utilizing SA to test ice crystal model phase functions has been previously given in Labonnote et al. (2001), but a brief description of this approach is given here. To compute SA the cloud bi-directional reflection, $\mathrm{R}(\mu,\, \mu_0,\, \phi\text{-}\phi_0)$, is found by:

$$\mathrm{R}(\mu, \mu_0, \phi\text{-}\phi_0) = \pi \mathrm{I}(\mu, \mu_0, \phi\text{-}\phi_0)/\mu_0 \mathrm{E}_0 \tag{2.11}$$

where $\mathrm{I}(\mu,\, \mu_0,\, \phi\text{-}\phi_0)$ is the reflected solar radiance from cloud-top, E_0 is the incident solar flux density, μ and μ_0 are cosines of the zenith view and solar zenith angles, respectively. The relative azimuth is given by $\phi\text{-}\phi_0$.

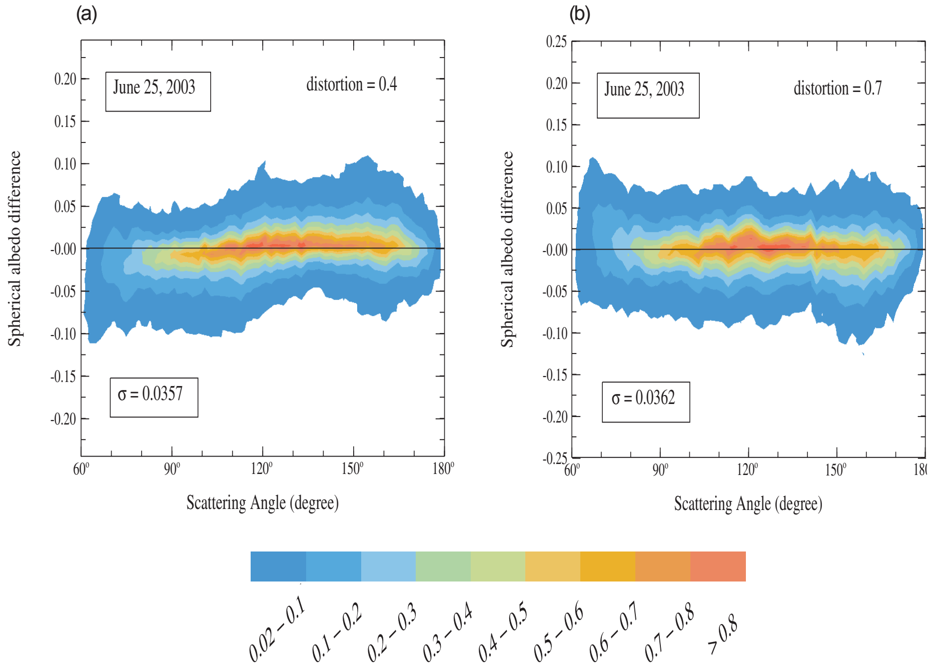

Fig. 2.14. Normalized density of selected pixel directions (the red colour represents more than 80% of the pixels) against scattering angle, showing differences between the retrieved spherical albedo obtained at the wavelength of 0.87 µm and the directionally averaged spherical albedo for the (a) chain-like hexagonal aggregate (Fig. 2.3 (g)) and (b) hexagonal ice aggregate (Fig. 2.3 (e)]. The assumed ice crystal parameters used in the calculations are given in Table 2.4. The degree of randomization is shown in the upper right-hand side of the figures and the standard deviation of the residual spherical albedo represented by σ is also shown in the figures (reproduced, with permission, from Baran and Labonnote, 2006).

Table 2.4. The physical dimensions of each ice crystal model assumed in the POLDER radiative transfer calculations

Model	Maximal dimension, µm
Six-branched bullet-rosette	100
Chain-like aggregate	100
Ice aggregate	100
Polycrystal	100
IHM	220

Eq. (2.11) can be integrated over all μ and ϕ-ϕ_0 to give the plane albedo, $\mathrm{A}(\mu_0)$, given by

$$A(\mu_0) = \frac{1}{\pi} \iint \mathrm{R}(\mu, \mu_0, \phi\text{-}\phi_0)\mu \,\mathrm{d}\mu \,\mathrm{d}\phi \tag{2.12}$$

and Eq. (2.12) can be integrated over all solar zenith angles to give the cloud spherical albedo (SA) a, given by

$$a = 2 \int \mathrm{A}(\mu_0)\mu_0 \,\mathrm{d}\mu_0 \tag{2.13}$$

The measurements of bi-directional reflectance at the wavelength of 0.670 µm are used to retrieve the cloud optical thickness in each viewing direction, which, assuming a black underlying surface, is equivalent to SA (see Doutriaux-Boucher et al., 2000; Labonnote et al., 2001). The measured SAs are simulated using a radiative transfer model based on the discrete-ordinates method due to Stamnes et al. (1988). The radiative transfer model assumes a homogeneous plane-parallel cloud and uses as input the satellite–Sun geometry, assumed ice crystal model phase function, the optical thickness, and the single scattering albedo, which is unity. If the phase function model were a perfect representation of scattering from cirrus then the retrieved SA would be independent of scattering angle. It is this aspect that Fig. 2.14 is testing.

The POLDER data shown in the figure was obtained during one day on the 25th June 2003 and the POLDER pixels were globally distributed and only pixels located over the sea were included. As can be seen from the figure both the randomized chain-like aggregate (Fig. 2.3 (g)) and randomized hexagonal ice aggregate (Fig. 2.3 (e)) do minimize the POLDER spherical albedo measurements well, with the standard deviations for each of the ice crystal models appearing quite similar. The reason for this similarity is that if the ice crystals are sufficiently randomized then the phase functions appear featureless, as shown in Fig. 2.9. However, the geometrical forms of each of the ice crystal models are very different, as shown in Fig. 2.3, but using reflection measurements alone is not sufficient to distinguish which of the randomized ice crystals best explains the POLDER measurements. However, the POLDER instrument also measures the polarized reflectance and, as shown in Fig. 2.10, polarization properties depend strongly on ice crystal shape. Perhaps this measurement can be used to distinguish between different types of randomized ice crystal? The results for the measured polarized reflectance assuming a variety of ice crystal models described in Fig. 2.3 are shown in Fig. 2.15 (a) and 2.15 (b) (from Baran and Labonnote (2006, Figs. 7a and Fig. 7b). Figure 2.15 (a) shows the POLDER-measured polarized reflectance plotted as a function of scattering angle with each of the ice crystal models with and without randomization represented by the various lines shown in the figure. The figure shows that when randomization is extreme the fit to the polarized reflection becomes worse; this is evident for the hexagonal ice aggregate and polycrystal models. However, the hexagonal ice aggregate did minimize the spherical albedo differences with such a randomization but this same model does not describe the POLDER-measured polarized

(a)

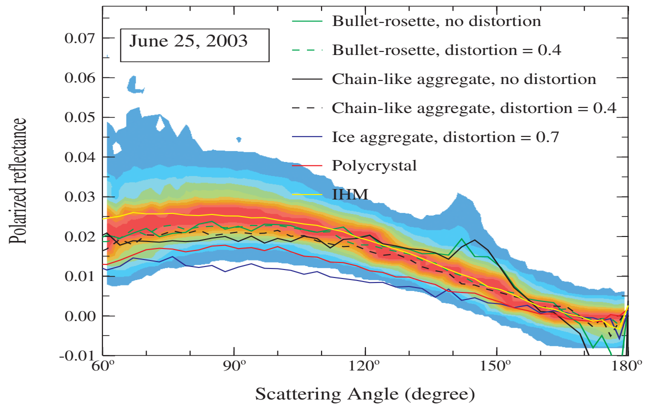

(b)

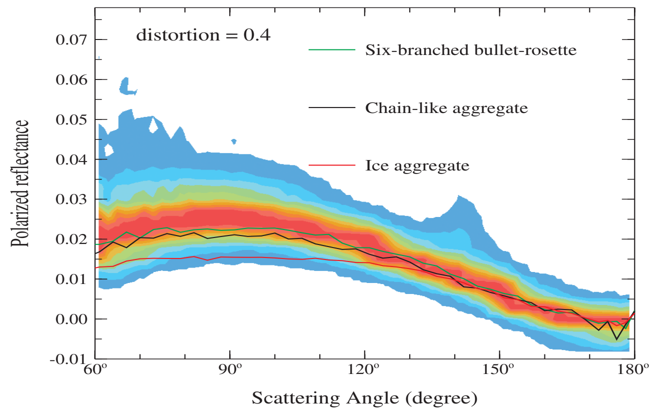

Fig. 2.15. (a) Same as Fig. 2.14 but for the polarized reflectance plotted against scattering angle for a variety of ice crystal models. The ice crystal parameters assumed in the calculations are given in Table 2.4. The ice crystals models are shown on the right-hand side of the figure together with the degree of distortion. (b) Same as (a) but for a single randomization showing polarization results for the six-branched bullet-rosette (green line), chain-like aggregate (black line), and the hexagonal ice aggregate (red line) (reproduced, with permission, from Baran and Labonnote, 2006).

reflectance. Therefore, in order to eliminate such models, intensity measurements alone are insufficient and additional information such as polarized reflectance is required.

Fig. 2.15 (b) shows that more spatial ice crystals such as the randomized chain-like aggregate and randomized bullet-rosette do satisfactorily explain the measured polarized reflectance, whilst more compact ice crystals such as the hexagonal ice aggregate do not. Again the geometrical form of the bullet-rosette and chain-like aggregate are very different (see Fig. 2.3), but not even a combination of reflection and polarized reflection can distinguish between them. The reason for this is that if sufficient randomization is applied to ice crystal models then all elements of the scattering matrix become featureless thus making distinction between more complex habits problematic. In order to distinguish between more complex randomized ice crystal models, further information is required, which could take the form of two-dimensional scattering patterns described by Ulanowski et al. (2006) or an enhanced version of the CPI. The utility of using the first three Stokes parameters (I, Q, and U) in the remote sensing of cirrus is further demonstrated by Ou et al. (2005). They show that by using simulated measurements at the wavelengths of 0.865 µm and 2.25 µm there is sensitivity to ice crystal shape, size and surface roughness.

2.5 Summary

This chapter has reviewed the current understanding of the optical and radiative properties of cirrus and it has demonstrated the importance of this cloud to climate modelling and remote sensing. The populations of nonspherical ice crystals that exist in cirrus are diverse; however, there is now sufficient evidence to say that pristine ice crystals such as hexagonal ice columns and hexagonal ice plates are uncommon. The most common nonspherical ice crystal type that inhabits synoptically generated cirrus is bullet-rosettes whilst anvil cirrus is mostly populated by non-symmetric irregulars. Representing these types of crystals by some geometric model such that the full single scattering properties can be solved is problematic. The current consensus appears to be that representing the variability of complex shapes by one single ice crystal model geometry does not appear to be supported either by *in situ* measurements of the IWC or airborne remote sensing of the scattering phase function. Representing the actual diversity of shapes by some ensemble model of ice crystal shapes, which are individually randomized, and that ensemble is able to replicate the measured IWC to a reasonable degree of accuracy is the better way forward. This approach reconciles the single scattering properties of the ensemble with macroscopic quantities such as IWC for any given particle size distribution function. This link between the cirrus single scattering properties and the amount of ice mass or IWC is the fundamental problem to be solved.

In recent years there have been significant advances in the development of electromagnetic methods to solve the single scattering properties of nonspherical ice crystals. This is especially true for the T-matrix and FDTD methods; however, there is still no one method that can solve the complete light scattering problem over the entire cirrus particle size distribution function. There is still reliance on approximations such as physical and geometric optics to bridge the gap between the so-called 'exact' methods and approximations. Though there are methods that can in principle be applied to any ice crystal shape given appropriate computational resources. The scattering properties of cirrus appear to be best represented by phase functions which are smooth and featureless; this is also true of the other elements of the scattering matrix. The reason for this featureless nature of the scattering phase function is due to the most common types of ice crystals having a non-symmetric form which may also be distorted or roughened, and/or contain inclusions of air or aerosol. In essence, the complete scattering properties from cirrus ice crystal ensembles are of a simple functional form, what is required is a computational method that can reproduce this simplicity from a given ensemble.

In order to solve the cirrus problem as outlined above, further airborne field campaigns are certainly required that are able to further quantify the cirrus particle size distribution function, and especially the role of small ice crystals less than 100 μm in size, and the most common geometrical form of these small ice crystals. Quantification of ice crystal shapes from different locations, heights and seasons, and instrumentation to measure their masses is also required. As regards airborne remote sensing, further measurements of the scattering phase function at non-absorbing and absorbing wavelengths over a wide range of scattering angle are needed. The development of high-resolution spectrometers that are able to measure cirrus radiances at both solar and infrared wavelengths simultaneously should enable rigorous testing of the modelled cirrus single scattering properties. As this chapter has shown, combining intensity measurements with polarization measurements is important when trying to distinguish between complex cirrus ice crystal models. However, as shown in this chapter, due to the simplicity of the scattering matrix elements for complex randomized ice crystals with very different geometrical forms, using both intensity and polarization to distinguish between such ice crystals is still problematic. For instance, it follows from Fig. 2.14 (a) (or Fig. 2.6 of Baran and Labonnote, 2006), and Fig. 2.15 that both the distorted chain-like aggregates (Fig. 2.3 (g)) and six-branched bullet-rosettes (Fig. 2.3 (d)) well represent the radiative and polarization properties of cirrus. These shapes are also similar to those shown in Fig. 2.1. Certainly, the use of intensity alone measurements is insufficient. Distinguishing between complex non-symmetric ice crystals might be achieved by using 2D scattering patterns or an enhanced version of the CPI. This distinction is important since at infrared wavelengths the absorption properties of different non-symmetric ice crystals will differ and will therefore not have the same radiative responses in climate models.

Acknowledgements

The author would like to thank A. J. Heymsfield for providing Fig. 2.1 and Fig. 2.2, P. N. Francis for providing the aircraft data, and C. Westbrook for providing Fig. 2.4. The UK Department of the Environment, Fisheries and Rural Affairs is also acknowledged for part supporting some of the work presented in this chapter.

References

Asano, S., and M. Sato, 1980: Light scattering by randomly oriented spheroidal particles, *Appl. Opt.*, **19**, 962–974.

Baran, A. J., P. D. Watts, and P. N. Francis, 1999: Testing the coherence of cirrus microphysical and bulk properties retrieved from dual-viewing multispectral satellite radiance measurements, *J. Geophys. Res.*, **104**, 31673–31683.

Baran, A. J., P. Yang, and S. Havemann, 2001a: Calculation of the single scattering properties of randomly oriented hexagonal ice columns: a comparison of the T-matrix and the finite-difference time-domain methods, Appl. Opt. **40**, 4376–4386.

Baran, A. J., P. N. Francis, L.-C. Labonnote, and M. Doutriaux-Boucher, 2001b: A scattering phase function for ice cloud: Tests of applicability using aircraft and satellite multi-angle multi-wavelength radiance measurements of cirrus, *Q. J. R. Meteorol. Soc.*, **127**, 2395–21416.

Baran, A. J., S. Havemann, P. N. Francis, and P. D. Watts, 2003: A consistent set of single scattering properties for cirrus cloud: A test using radiance measurements from a dual-viewing multi-wavelength satellite-based instrument, *J. Quant. Spectr. Rad. Transfer*, **79–80**, 549–567.

Baran, A. J., 2003a: On the scattering and absorption properties of cirrus cloud, *J. Quant. Spectr. Rad. Transfer*, **89**, 17–36.

Baran, A. J., 2003b: Simulation of infrared scattering from ice aggregates by use of a size-shape distribution of circular ice cylinders, *Appl. Opt.*, **42**, 2811-2818.

Baran, A. J., and S. Havemann, 2004: The dependence of retrieved ice-crystal effective dimension on assumed ice crystal geometry and size-distribution function at solar wavelengths, *Q. J. R. Meteorol. Soc.*, **130**, 2153–2167.

Baran, A. J., and P. N. Francis, 2004: On the radiative properties of cirrus cloud at solar and thermal wavelengths: A test of model consistency using high-resolution airborne radiance measurements, *Q. J. R. Meteorol. Soc.*, **130**, 763–778.

Baran, A. J., 2005: The dependence of cirrus infrared radiative properties on ice crystal geometry and shape of the size-distribution function, *Q. J. R. Meteorol. Soc.*, **131**, 1129–1142.

Baran, A. J., V. N. Shcherbakov, B. A. Baker, J. F. Gayet and R. P. Lawson, 2005: On the scattering phase-function of non-symmetric ice crystals, *Q. J. R. Meteorol. Soc.*, **131**, 2609–2616.

Baran A. J., and L. C. Labonnote, 2006. On the reflection and polarization properties of ice cloud, *J. Quant. Spectrosc. Radiat. Transfer*, **100**, 41–54.

Baran, A. J., 2006: The suitability of assuming ice aggregates as a predictor of ice water content, *OBR Tech. Note. No. 56*, Met Office, Exeter.

Baum, B. A., D. P. Kratz, P. Yang, S. C. Ou, Y. X. Hu, P. F. Soulen, and S. C. Tsay, 2000: Remote sensing of cloud properties using MODIS airborne simulator imagery during SUCCESS 1. Data and models, J. Geophys. Res. **105**, 11767–11780.

Baum, B. A., A. J. Heymsfield, P. Yang, and S. T. Bedka, 2005: Bulk scattering properties for the remote sensing of ice clouds. Part I. Microphysical data and models, *J. App. Met.*, **44**, 1885–1895.

Borovoi, A., I. Grishin, E. Naats, and U. Oppel, 2000: Backscattering peak of hexagonal ice columns and plates, *Opt. Lett.*, **25**, 1388-1392.

Borovoi, A. G., and I. A. Grishin, 2003: Scattering matrices for large ice crystal particles, *JOSA*, **A 20**, 2071–2080.

Borovoi, A., A. Cohen, N. Kustova, and U. Oppel, 2005: Light scattering by large ice crystal particles, Proc. 8th *Conference on Electromagnetic and Light Scatter-*

ing by Nonspherical Particles: Theory, Measurements and Applications, Salobreña, Granada, Spain, May 16th–20th, 44–47.

Bréon, F.-M., and B. Dubrulle, 2004: Horizontally oriented plates in clouds, *J. Atmos. Sci.*, **61**, 2888–2898.

Bryant, F. D., and P. Latimer, 1969: Optical efficiencies of large particles of arbitrary shape and orientation, *J. Colloid Interface Sci.*, **30**, 291–304.

Buriez, J.-C., C. Vanbauce, F. Parol, P. Gouloub, M. Herman, B. Bonnel, Y. Fouquart, P. Couvert, and G. Séze, 1997: Cloud detection and derivation of cloud properties from POLDER, *Int. J. Remote. Sensing*, **18**, 2785-2813.

Cai, Q., and K. N. Liou, 1982: Polarized light scattering by hexagonal ice crystals: Theory, *Appl. Opt.*, **21**, 3569–3580.

Chepfer, H., G. Brogniez, P. Goloub, F. M. Bréon, and P. H. Flamant, 1999: Observations of horizontally oriented ice crystals in cirrus clouds with POLDER-1/ADEOS-1, *J. Quant. Spectr. Rad. Transfer*, **63**, 521–543.

Clarke, A. J. M., E. Hesse, Z. Ulanowski, and P. H. Kaye, 2006: A 3D implementation of ray tracing combined with diffraction on facets: Verification and a potential application, *J. Quant. Spectrosc. Radiat. Transfer*, **100**, 103–114.

Connolly, P. J., C. P. R. Saunders, M. W. Gallagher, K. N. Bower, M. J. Flynn, T. W. Choularton, J. Whiteway, and R. P. Lawson, 2004: Aircraft observations of the influence of electric fields on the aggregation of ice crystals, *Q. J. R. Meteorol. Soc.*, **128**, 1-1-9.

Donner, L., C. J. Seman, B. J. Soden, R. S. Hemler, J. C. Warren, J. Strom, and K. N. Liou, 1997: Large-scale ice clouds in the GFDL SKYHI general circulation model, *J. Geophys. Res.*, **102**, 460–470.

Doutriaux-Boucher, M., J.-C. Buriez, G. Brogniez, L.-C. Labonnote, and A. J. Baran, 2000: Sensitivity of retrieved POLDER directional cloud optical thickness to various ice particle models, Geophys. *Res. Lett.*, **27**, 109–112.

Edwards, J. M., and A. Slingo, 1996: Studies with a flexible new radiation code. 1. Choosing a configuration for a large-scale model, Q. J. R. Meteorol. Soc. **122**, 689–719.

Edwards, J. M., S. Havemann, J.-C. Thelen, and A. J. Baran, 2007: A new parametrization for the radiative properties of ice crystals: Comparison with existing schemes and impact in a GCM, *Atmos. Res.*, **83**, 19–34.

Field, P. R., A. J. Baran, P. H. Kaye, E. Hirst, and R. Greenway, 2003: A test of cirrus ice crystal scattering phase functions, *Geophys. Res. Lett.*, **30**, 1752, doi: 10.1029/2003GL017482.

Field, P. R., R. J. Hogan, P. R. A. Brown, A. J. Illingworth, T. W. Choularton, and R. J. Cotton, 2005: Parametrization of ice-particle size distribution functions for mid-latitude stratiform cloud, *Q. J. R. Meteorol. Soc.*, **131**, 1997–2017.

Foot, J., 1988: Some observations of the optical properties of clouds. II: Cirrus, *Q. J. R. Meteorol. Soc.*, **114**, 141–164.

Francis, P. N., A. Jones, R. W. Saunders, K. P. Shine, A. Slingo, and Z. Sun, 1994: An observational and theoretical study of the radiative properties of cirrus: Some results from ICE'89, *Q. J. R. Meteorol. Soc.*, **120**, 809–848.

Francis, P. N., J. S. Foot, and A. J. Baran, 1999: Aircraft measurements of the solar and infrared radiative properties of cirrus and their dependence on ice crystal shape, *J. Geophys. Res.*, **104**, 31685–31695.

Fu, Q., 1996: An accurate parameterization of the solar radiative properties of cirrus clouds for climate models, *J. Climate*, **9**, 2058–2082.

Fu, Q., W. B. Sun, and P. Yang, 1999: Modeling of scattering and absorption by nonspherical cirrus ice particles at thermal infrared wavelengths, *J. Atmos. Sci.*, **56**, 2937–2947.

Gallagher, M. W., J. Whiteway, M. J. Flynn, P. J. Connolly, D. Figueros-Nieto, T. W. Choularton, K. N. Bower, C. Cook, R. Busen, and J. Hacker, 2004: An overview of the microphysical structure of cirrus clouds observed during emerald-1, *Q. J. R. Meteorol. Soc.*, **131**, 1143–1169.

Garrett, T. J., H. Gerber, D. G. Baumgardner, C. H. Twohy, and E. M. Weinstock, 2003: Small, highly reflective ice crystals in low-latitude cirrus, *Geophys. Res. Lett.*, **30**, Art. No. 2132.

Garrett, T. J., B. C. Navarro, C. H. Twohy, E. J. Jensen, D. G. Baumgardner, P. T. Bui, H. Gerber, R. L. Herman, A. J. Heymsfield, P. Lawson, P. Minnis, L. Nguyen, M. Poellot, S. K. Pope, F. P. J. Valero, and E. M. Weinstock, 2005: Evolution of a Florida anvil, *J. Atmos. Sci.*, **62**, 2352–2372.

Gerber H., Y. Takano, T. J. Garrett, P. V. Hobbs, 2000: Nephelometer measurements of the asymmetry parameter, volume extinction coefficient, and backscatter ratio in Arctic clouds, *J. Atmos. Sci.*, **57**, 3021–3034.

Hartmann, D. L., M. E. Ockert-Bell, and M. L. Michelsen, 1992: The effect of cloud type on earth's energy balance: Global analysis, *J. Clim.*, **5**, 1281–1304.

Havemann, S., A. J. Baran, and J. M. Edwards, 2003: Implementation of the T-matrix method on a massively parallel machine: A comparison of hexagonal ice cylinder single scattering properties using the T-matrix and improved geometric optics methods, *J. Quant. Spectr. Rad. Transfer*, **79–80**, 707–720.

Henyey, L., and J. Greenstein, 1941: Diffuse radiation in the galaxy, *Astrophys. Journal*, **93**, 70–83.

Hesse, E., and Z. Ulanowski, 2003: Scattering from long prisms computed using ray tracing combined with diffraction on facets, *J. Quant. Spectr. Rad. Trans.*, **79–80**, 721–732.

Hesse, E., Z. Ulanowski, and S. Havemann, 2003: Scattering from long prisms: a comparison between ray tracing combined with diffraction on facets and SVM, In *Proc 7th Int. Conf. on Electromagnetic and Light Scattering bu Bon-spherical particles*, Bremen, 119–122.

Heymsfield, A. J., and C. M. R. Platt, 1984: A parametrization of the particle size spectrum of ice clouds in terms of the ambient temperature and ice water-content, *J. Atmos. Sci.*, **41**, 846–855.

Heymsfield, A. J., A. Bansemer, P. R. Field, S. L. Durden, J. L. Stith, J. E. Dye, W. Hall, C. A. Grainger, 2002: Observations and parameterizations of particle size distributions in deep tropical cirrus and stratiform precipitating clouds: Results from in situ observations in TRMM field campaigns, *J. Atmos. Sci.*, **59**, 3457–3491.

Heymsfield, A. J., and L. M. Miloshevich, 2003. Parametrizations for the cross-sectional area and extinction of cirrus and stratiform ice cloud particles, *J. Atmos. Sci.*, **60**, 936–956.

Hong, G., G. Heygster, and C. A. M. Rodriguez, 2006: Effect of cirrus clouds on the diurnal cycle of tropical deep convective clouds, *J. Geophys. Res.*, **111**, D06209, doi:10.1029/2005JD006208.

IPCC, 2001: Climate change 2001: The scientific basis. Third assessment report of the Intergovernmental Panel on Climate Change, Eds. J. T. Houghton, Y. Ding, D. J. Griggs, M. Noguer, P. J. Van der Linden, X. Dai, K. Maskell and C. A. Johnson, Cambridge University Press, Cambridge and New York.

Ivanova, D., D. L. Mitchell, W. P. Arnott, and M. Poellot, 2001: A GCM parameterization for bimodal size spectra and ice mass removal rates in mid-latitude cirrus clouds, *Atmos. Res.*, **59**, 89–113.

Kahnert, F. M., J. J. Stamnes, and K. Stamnes, 2001: Application of the extended boundary condition method to particles with sharp edges: a comparison of two surface integration approaches, *Appl. Opt.*, **40**, 3101–3109.

Kahnert, F. M., J. J. Stamnes, and K. Stamnes, 2002a: Can simple particle shapes be used to model scalar optical properties of an ensemble of wavelength-sized particles with complex shapes, *J. Opt. Soc. Am.*, **A 19**, 521–531.

Kahnert, F. M., J. J. Stamnes, and K. Stamnes, 2002b: Using simple particle shapes to model the stokes scattering matrix of ensembles of wavelength-sized particles with particles with complex shapes: possibilities and limitations, *J. Quant. Spectr. Rad. Transfer*, **74**, 167–182.

Kahnert, F. M., 2003: Numerical methods in electromagnetic scattering theory, *J. Quant. Spectrosc. Radiat. Transfer*, **79–80**, 775–824.

Kite, A. J., 1987: The albedo of broken cloud fields, *Q. J. R. Meteorol. Soc.*, **113**, 517–531.

Kokhanovsky, A., and A. Macke, 1997: The dependence of the radiative characteristicss of optically thick media on the shape of particles, *J. Quant. Spectr. Rad. Transfer*, **63**, 393–407.

Kokhanovsky, A., 2004: Optical properties of terrestrial clouds, *Earth Sci. Revs.*, **64**, 189–241.

Kokhanovsky, A., 2005a: Phase matrix of ice crystals in noctilucent clouds, *Proc. SPIE*, **5829**, 44–52.

Kokhanovsky, A., 2005b: Microphysical and optical properties of noctilucent clouds, *Earth Sci. Rev.*, **71**, 127–146.

Kokhanovsky, A., 2006: Modeling of light depolarization by cubic and hexagonal particles in noctilucent clouds, *Atmos. Res.*, **79**, 175–181.

Korolev, A., G. A. Isaac, and J. Hallett, 2000: Ice particle habits in stratiform clouds, *Q. J. R. Meteorol. Soc.*, **126**, 2873–2902.

Kristjánsson, J. E., J. M. Edwards, and D. L. Mitchell, 2000: The impact of a new scheme for the optical properties of ice crystals on the climate of two GCMs, *J. Geophys. Res.*, **105**, 10063–10079.

Labonnote, L.-C., G. Brogniez, J. C. Buriez, M. Doutriaux-Boucher, J. F. Gayet, and A. Macke, 2001: Polarized light scattering by inhomogeneous hexagonal monocrystals: Validation with ADEOS-POLDER measurements, *J. Geophys. Res.*, **106**, 12139–12153.

Lawson, P., B. A. Baker, C. G. Schmitt, T. L. Jensen, and K. N. Liou, 2001: An overview of microphysical properties of artic clouds observed in May and July 1998 during fire ace, *J. Geophys. Res.*, **106**, 14989–15014.

Lawson, P., B. A. Baker, and B. L. Pilson, 2003: In situ measurements of microphysical properties of mid-latitude and anvil cirrus and validation of satellite retrievals, In *Proc 30th International Symposium on Remote Sensing of Environment*. Honolulu, Hawaii.

Lee, Y. K., P. Yang, M. I. Mishchenko, B. A. Baum, Y. X. Hu, H. L. Huang, W. J. Wiscombe, and A. J. Baran, 2003: Use of circular cylinders as surrogates for hexagonal pristine ice crystals in scattering calculations at infrared wavelengths, *Appl. Opt.*, **42**, 2653–2664.

Liou, K. N., 1986: Influence of cirrus clouds on weather and climate process: A global perspective, *Mon. Weather Rev.*, **114**, 1167–1199.

Liou, K. N., and Y. Takano, 1994: Light scattering by nonspherical particles: Remote sensing and climatic implications, *Atmos. Res.*, **31**, 271–298.

Liou, K. N., Y. Takano, and P. Yang, 2000: Light scattering and radiative transfer by ice crystal clouds: Applications to climate research, in *Light Scattering by Nonspherical Particles: Theory, Measurements, and Geophysical Applications*, Eds. M. I. Mishchenko, J.W. Hovenier, and L. D. Travis, Academic Press, San Diego, CA, 417–449.

Lohmann, U., and E. Roeckner, 1995: Influence of cirrus radiative forcing on climate and climate sensitivity in a general-circulation model, *J. Geophys. Res.*, **100**, 16305–16323.

Lynch, D., K. Sassen, D. Star and G. L. Stephens (Eds.), 2002: *Cirrus*, Oxford University Press, Oxford.

Macke, A., 1993: Scattering of light by polyhedral ice crystals, *Appl. Opt.*, **32**, 2780–2788.

Macke, A. J. Mueller, and E. Raschke, 1996: Single scattering properties of atmospheric ice crystal, *J. Atmos. Sci.*, **53**, 2813–2825.

Mackowski, D. W., 2002: Discrete dipole moment method for calculation of the T matrix for nonspherical particles, *J. Opt. Soc. Am.*, **A 19**, 881–893.

Mano, Y., 2000: Exact solution of electromagnetic scattering by a three-dimensional hexagonal ice column obtained with the boundary-element method, *Appl. Opt.*, **39**, 5541–5546.

McFarlane, S. A., R. T. Marchand, and T. P. Ackerman, 2005: Retrieval of cloud phase and crystal habit from multiangle imaging spectroradiometer (MISR) and moderate resolution imaging spectroradiometer (MODIS) data, *J. Geophys. Res.*, **110**, D14201, doi:10.1029/2004JD004831.

McFarquhar, G. M., and A. J. Heymsfield, 1996: Microphysical characteristics of three anvils sampled during the central equatorial pacific experiment, *J. Atmos. Sci.*, **53**, 2401–2423.

McFarquhar, G. M., and A. J. Heymsfield, 1998: The definition and significance of an effective radius for ice clouds, *J. Atmos. Sci.*, **55**, 2039–2052.

McFarquhar, G. M., A. J. Heymsfield, A. Macke, J. Iaquinta, and S. M. Aulenbach, 1999: Use of observed ice crystal sizes and shapes to calculate the mean-scattering properties and multispecrtral radiance, CEPEX April 4 1993 case study, *J. Geophy. Res.*, **104**, 31763–31779.

McFarquhar, G. M., P. Yang, A. Macke and A. J. Baran, 2002: A new parameterization of single scattering solar radiative properties for tropical anvils using observed ice crystal size and shape distributions, *J. Atmos. Sci.*, **59**, 2458–2478.

Mishchenko, M. I., and A. Macke, 1997: Asymmetry parameters of the phase function for isolated and densely packed spherical particles with multiple internal inclusions in the geometric optics limit, *J. Quant. Spectr. Rad. Transfer*, **57**, 767–794.

Mishchenko, M. I., and L. D. Travis, 1998: Capabilities and limitations of a current FORTRAN implementation of the T-matrix method for randomly oriented, rotationally symmetry scatterers, *J. Quant. Spectrosc. Radiat. Transfer*, **60**, 309–324.

Mishchenko, M. I., L. D. Travis, and A. A. Lacis, 2002: *Scattering, Absorption, and Emission of Light by Small Particles*, Cambridge University Press, Cambridge, UK.

Mitchell, J. F. B., C. A. Senior, and W. J. Ingram, 1989: CO2 and climate: A missing feedback? *Nature*, **341**, 132–134.

Mitchell, D. L., and W. P. Arnott, 1994: A model predicting the evolution of ice particle size spectra and radiative properties of cirrus clouds, II, Dependence of absorption and extinction on ice crystal morphology, *J. Atmos. Sci.*, **51**, 817–832.

Mitchell, D. L., Y. Liu, and A. Macke, 1996: Modeling cirrus clouds. Part II: Treatment of radiative properties, *J. Atmos. Sci.*, **53**, 2967–2988.

Mitchell, D. L., W. P. Arnott, C. Schmitt, A. J. Baran, S. Havemann, and Q. Fu, 2001: Photon tunneling contributions to extinction for laboratory grown hexagonal columns, *J. Quant. Spectr. Rad. Transfer*, **70**, 761–776.

Mitchell, D. L., 2002: Effective diameter in radiation transfer, *J. Atmos. Sci.*, **59**, 2330–2346.

Mitchell, D. L., A. J. Baran, W. P. Arnott, and C. Schmitt, 2006: Testing and comparing the Modified Anomalous Diffraction Approximation, *J. Atmos. Sci.*, **63**, 2948–2962.

Muinonen, K., 1989: Scattering of light by crystals: a modified Kirchhoff approximation, *Appl. Opt.*, **28**, 3044–3050.

Noel, V., and H. Chepfer, 2004: Study of ice crystal orientation in cirrus clouds based on satellite polarized radiance measurements, *J. Atmos. Sci.*, **61**, 2073–2081.

Nousiainen, T., and G. M. McFarquhar, 2004: Light scattering by small quasi-spherical ice crystals, *J. Atmos. Sci.*, **61**, 2229–2248.

Ou, S. C., K. N. Liou, Y. Takano, and R. L. Slonaker, 2005: Remote sensing of cirrus cloud particle size and optical depth using polarimetric sensor measurements, *J. Atmos. Sci.*, **62**, 4371–4383.

Ringer, M. A., J. M. Edwards, and A. Slingo, 2003: Simulation of satellite channel radiances in the Met Office Unified Model, *Q. J. R. Meterol. Soc.*, **129**, 1169–1190.

Rolland, P., K. N. Liou, M. D. King, S. C. Tsay, and G. M. McFarquhar, 2000: Remote sensing of optical and microphysical properties of cirrus clouds using MODIS channels: methodology and sensitivity to assumptions, *J. Geophys. Res.*, **105**, 11,721–11,738.

Rother, T., K. Schmidt, and S. Havemann, 2001: Light scattering on hexagonal ice columns, *J. Opt. Soc. Am*, **A 18**, 2512–2517.

Saunders, C. P. R., and N. M. A. Wahab, 1975: The influence of electric fields on the aggregation of ice crystals, *J. Meteorol. Soc. Japan*, **53**, 121–126.

Slingo, A., 1989: A GCM parameterization for the shortwave radiative properties of water clouds, *J. Atmos. Sci.*, **46**, 1419–1427.

Stamnes, K., S.-C. Tsay, W. Wiscombe, and K. Jayaweera, 1988: Numerically stable algorithm for discrete-ordinate-method radiative transfer in multiple scattering and emitting layered media, *Appl. Opt.*, **27**, 2502–2509.

Stephens, G. L., and P. J. Webster, 1981: Clouds and climate: sensitivity of simple systems, *J. Atmos. Sci.*, **38**, 235–247.

Stephens, G. L., S.-C. Tsay, P. W. Stackhous, and P. J. Flatau, 1990: The relevance of the microphysical and radiative properties of cirrus clouds to climate and climate feedback, *J. Atmos. Sci.*, **47**, 1742–1753.

Sun, W. B., Q. Fu, and Z. Chen, 1999: Finite-difference time-domain solution of light scattering by dielectric particles with perfectly matched layer absorbing boundary conditions, *Appl. Opt.*, **38**, 3141–3151.

Sun, W. B., and Q. Fu, 2001: Anomalous diffraction theory for randomly oriented nonspherical particles: A comparison between original and simplified solutions, *J. Quant. Spectr. Rad. Transfer*, **70**, 737–747.

Sun, W. B., T. Nousiainen, K. Muinonen, Q. Fu, N. G. Loeb, and G. Videen, 2003: Light scattering by Gaussian particles: a solution with finite-difference time-domain technique, *J. Quant. Spectr. Rad. Transfer*, **79**, 1083–1090.

Sun, W. B., N. G. Loeb, G. Videen, and Q. Fu, 2004: Examination of surface roughness on light scattering by long ice columns by use of a two-dimensional finite-difference time-domain algorithm, *Appl. Opt.*, **43**, 1957–1964.

Takano, Y., and K. N. Liou, 1989a: Solar radiative transfer in cirrus clouds. Part I. Single-scattering and optical properties of hexagonal ice crystals, *J. Atmos. Sci.*, **46**, 3–19.

Takano, Y., and K. N. Liou, 1989b: Radiative transfer in cirrus clouds. II. Theory and computation of multiple scattering in an anisotropic medium, *J. Atmos. Sci.*, **46**, 20–36.

Ulanowski, Z., E. Hesse, P. H. Kaye and A. J. Baran, 2006: Light scattering by complex ice-analogue crystals, *J. Quant. Spectr. Rad. Transfer*, **100**, 382–392.

van de Hulst, H. C., 1957: Light Scattering by Small Particles, Wiley, New York.

Volkovitskiy, O. A., L. N. Pavlova, and A G. Petrushin, 1980: Scattering of light by ice crystals, *Atmos. Ocean. Phys.*, **16**, 90–102.

Wahab, N. M. A., 1974: Ice crystal interactions in electric fields, Ph.D. thesis, UMIST.

Warren, S. G. 1984: Optical constants of ice from the ultraviolet to the microwave, *Appl. Opt.*, **23**, 1206–1224.

Wendling, P., R. Wendling, and H. K. Weickmann, 1979: Scattering of solar radiation by hexagonal ice crystals, *Appl. Opt.*, **18**, 2663–2671.

Westbrook, C. D., R. C. Ball, P. R. Field, and A. J. Heymsfield, 2004: Theory of growth by differential sedimentation, with application to snowflake formation, *Phys. Rev. E*, **70**, Art. No. 021403.

Wylie, D. P., W. P. Menzel, H. M. Woolf, and K. I. Strabala, 1994: Four years of global cirrus statistics using HIRS, *J. Climate*, **7**, 1972–1986.

Wyser, K., and P. Yang, 1998: Average ice crystal size and bulk short-wave single scattering properties of cirrus clouds, *Atmos. Res.*, **49**, 315–335.

Yang, P., and K. N. Liou, 1995: Light scattering by hexagonal ice crystals: Comparison of finite-difference time domain and geometric optics methods, *J. Opt. Soc. Amer. A*, **12**, 162–176.

Yang, P., and K. N. Liou, 1996: Geometric-optics-integral-equation method for light scattering by nonspherical ice crystals, *Appl. Opt.*, **35**, 6568–6584.

Yang, P., K. N. Liou, and W. P. Arnott, 1997: Extinction efficiency and single scattering albedo for laboratory and natural cirrus clouds, *J. Geophys. Res.*, **102**, 21825-21835.

Yang, P., and K. N. Liou, 1998: Single-scattering properties of complex ice crystals in terrestrial atmosphere, *Contr. Atmos. Phys.*, **71**, 223–248.

Yang, P., K. N. Liou, M. I. Mishchenko, and B.-C. Gao, 2000: An efficient finite-difference time domain scheme for light scattering by dielectric particles: Application to aerosols, *Appl. Opt.*, **39**, 3727–3737.

Yang, P., B.-C. Gao, B. A. Baum, W. Wiscombe, Y. Hu, S. L. Nasiri, A. Heymsfield, G. McFarquhar, and L. Miloshevich, 2001: Sensitivity of cirrus bidirectional reflectance in MODIS bands to vertical inhomogeneity of ice crystal habits and size distributions, *J. Geophys. Res.*, **106**, 17267-17291.

Yang, P., B. A. Baum, A. J. Heymsfield, Y. X. Hu, H.-L. Huang, S.-Chee Tsay, and S. Ackerman, 2003: Single-scattering properties of droxtals, *J. Quant. Spectrosc. Radiat. Transfer*, **79–80**, 1159–1180.

Yang, P., G. W. Kattawar, and W. J. Wiscombe, 2004: Effect of particle asphericity on single scattering parameters: Comparison between Platonic solids and spheres, *Appl. Opt.*, **43**, 4427–4435.

Zhang, Y., A. Macke, and F. Albers, 1999: Effect of crystal size spectrum and crystal shape on stratiform cirrus radiative forcing, *Atmos. Res.*, **52**, 59–75.